



Review

Atomic force microscopy for the investigation of molecular and cellular behavior



Alper D. Ozkan, Ahmet E. Topal, Aykutlu Dana, Mustafa O. Guler, Ayse B. Tekinay*

Bilkent University, UNAM-Institute of Materials Science and Nanotechnology, Ankara, Turkey

ARTICLE INFO

Article history:

Received 4 May 2016

Accepted 27 July 2016

Available online 29 July 2016

Keywords:

Atomic force microscopy

Biomacromolecules

Mechanical characterization

Cells

ABSTRACT

The present review details the methods used for the measurement of cells and their exudates using atomic force microscopy (AFM) and outlines the general conclusions drawn by the mechanical characterization of biological materials through this method. AFM is a material characterization technique that can be operated in liquid conditions, allowing its use for the investigation of the mechanical properties of biological materials in their native environments. AFM has been used for the mechanical investigation of proteins, nucleic acids, biofilms, secretions, membrane bilayers, tissues and bacterial or eukaryotic cells; however, comparison between studies is difficult due to variances between tip sizes and morphologies, sample fixation and immobilization strategies, conditions of measurement and the mechanical parameters used for the quantification of biomaterial response. Although standard protocols for the AFM investigation of biological materials are limited and minor differences in measurement conditions may create large discrepancies, the method is nonetheless highly effective for comparatively evaluating the mechanical integrity of biomaterials and can be used for the real-time acquisition of elasticity data following the introduction of a chemical or mechanical stimulus. While it is currently of limited diagnostic value, the technique is also useful for basic research in cancer biology and the characterization of disease progression and wound healing processes.

© 2016 Elsevier Ltd. All rights reserved.

Contents

1. Introduction	60
2. Effect of probe morphology, composition and surface chemistry	61
3. Atomic force microscopy of unicellular organisms	62
3.1. Bacterial cell surfaces	62
3.2. Bacterial secretions, exudates and biofilms	64
4. Atomic force microscopy of mammalian cells and tissues	64
4.1. Cancer diagnosis and characterization	67
4.2. Diagnosis of other diseases	69
4.3. Stem cell differentiation	70
4.4. Extracellular secretions and tissue microenvironments	71
5. Future directions	71
References	73

1. Introduction

Both uni- and multicellular organisms coordinate their behavior using a network of chemical, electrical and mechanical signals, and employ a variety of sensory mechanisms to perceive and respond

to internal or external regulatory cues (Ricca et al., 2013; Johnson, 2013). In unicellular organisms, such signals may assist in feeding, attracting conspecifics, synchronizing reproductive cycles or initiating defense mechanisms in a hostile environment (Dufour and Levesque, 2013); while multicellular life utilizes cell signaling networks to regulate cell recruitment, adhesion, differentiation, proliferation and death (Watt and Huck, 2013; Ravichandran, 2003; Zoranovic et al., 2013; Jaenisch and Bird, 2003; Owens and Wise, 1997). As the latter category of processes are integral to sustain complex life, the characterization of regulatory signals is of great

* Corresponding author.

E-mail address: atekinay@bilkent.edu.tr (A.B. Tekinay).

importance to the medical and biological sciences, and much work has been performed to elucidate the links between environmental cues and cellular processes (Ando et al., 2013; Carvalho et al., 2013; Dorobantu et al., 2012). However, while the chemical and biological environment of cells are relatively well-defined, the mechanical properties of cells and their immediate environment are investigated only to a lesser degree; partly because of the high complexity and variability of the mechanical interactions exhibited by cells and partly due to limitations associated with the high-resolution mechanical probing of cell surfaces and interiors (Cohen and Kalfon-Cohen, 2013). Nonetheless, considerable effort has been spent to establish how cells perceive and act upon the physical characteristics of nearby substrates (Shao et al., 1996), and to determine how the mechanical properties of cells and tissues are altered in response to disease state or environmental factors, using material characterization tools such as magnetic twisting cytometry, optical tweezers, microneedle probes, scanning acoustic microscopy and atomic force microscopy (Neuman and Nagy, 2008).

Atomic force microscopy (AFM) is a characterization tool that measures the topology and material properties of surfaces by recording the deflection of a metallic probe (or "tip") as it moves over the target surface. AFM can be operated under three principal modes: In contact mode, the tip is dragged directly over the surface and deflects away due to a repulsive Coulombic interaction, while in non-contact mode it is held at a short (typically <100 nm) distance over the sample and oscillates at a frequency that depends on the attractive van der Waals forces acting upon it. In tapping or intermittent contact mode, the tip is kept oscillating above the sample, and the oscillation frequency changes as the tip approaches the surface at regular intervals (Giessibl, 2003). Contact and intermittent modes are particularly suitable for the probing of biological samples, due to their applicability in liquid media (Danino, 2008). Despite considerable losses in resolution, a liquid sample environment allows cellular imaging in a native (or pseudo-native) environment and, more importantly, permits the direct investigation of mechanical changes on a live cell surface in response to an introduced stimulus (Liu et al., 2005). Time-lapse elastographs taken in this fashion have been utilized for a diverse array of applications, including to visualize the formation of amyloid (Harper et al., 1997) or collagen (Revenko et al., 1994) fibers under different environmental conditions, determine how membrane integrity is altered in the presence of antibiotics (Fantner et al., 2010a), or record the production and dissolution of cytoskeletal elements during cell movement (Rotsch and Radmacher, 2000). In addition, it is possible to utilize the AFM tip as a stimulus to elicit a response from the target cell, and the probe itself can be functionalized with ligand molecules to determine the affinity of the cell membrane to a particular biological moiety.

Due to the versatility and potential application areas of AFM, the technique has attracted substantial interest in biomechanical research, and has been used in the characterization of a great variety of tissues, cells and sub-cellular structures in both live condition and following fixing and drying. The present review aims to cover those studies that focus on the differences in mechanical properties associated with pathological conditions or changes in environmental cues, and emphasizes the importance of the mechanical Umwelt in modulating the behavior of both single-celled and multicellular systems.

2. Effect of probe morphology, composition and surface chemistry

Before discussing the AFM imaging of biological materials, the importance of AFM tip choice should be underlined. The diameters, materials, morphologies and cantilever lengths of commercial

AFM probes show considerable variance, and optimal performance requires the use of a probe conducive to the task at hand. The composition of the sample material should be taken into consideration to choose the spring constant of the AFM probe, as softer materials, such as cells, may be damaged over repeated contact with the AFM tip (Costa, 2003). In addition, depending on the area to be scanned, it may be desirable to increase or decrease the tip diameter. Larger tips are associated with lower resolution, but can be utilized to scan larger sample areas without compromising tip integrity, as sharper tips may experience significant wear over long scanning distances, such as when scanning cells. On the other hand, sharper tips are capable of resolving smaller features to a greater extent, which is invaluable when measuring proteins and other nanoscale biological materials. Consequently, differences in material stiffness that are evident under nanoscale investigation may be unmeasurable using microscale tips (Stoltz et al., 2009a). If adhesion data is to be collected, the material and morphology of the AFM tip (alongside substrate properties) also determines the suitable model for use in elasticity calculations (Fig. 1).

AFM probes can also be functionalized in order to characterize the interaction between two specific types of biological moieties, such as between a receptor and its ligand. This type of interaction is best exemplified by biotin and avidin, used by Colton et al. in their hallmark paper to illustrate the possibility of using AFM to directly evaluate the strength of molecular interactions (Lee et al., 1994). Mechanical properties of a wide variety of proteins have now been elucidated, including the interactions between antibodies and their corresponding antigens (Allen et al., 1997), actin and myosin (Kodera et al., 2010), osteopontin and integrin (Lee et al., 2007), and various cell adhesion proteoglycans (Dammer et al., 1995). Such proteins can either be covalently tethered to the target material (Ebner et al., 2007; Kamruzzahan et al., 2006) or attached by drying the protein sample on the surface (Florin et al., 1995). In addition, the mechanical strength of the constituent domains of a single protein can be evaluated by attaching that protein to a surface and using the AFM tip to stretch it (Li et al., 2003). This results in the gradual unfolding of the protein, and the unwinding of each domain is associated with a momentary drop in force. Tensile characteristics of the immunoglobulin and fibronectin III domains of titin were investigated using this method (Rief et al., 1998), and the ability of the bacterial ribonuclease barnase to withstand force was likewise evaluated by incorporating this protein into a chimeric construct consisting of four TI I27 and three barnase subunits (Best et al., 2001).

DNA and RNA can also be immobilized and characterized in a similar manner, and the mechanical investigation of DNA molecules of varying lengths and configurations has been performed using AFM (Mao et al., 1999; Hansma et al., 1995). In addition to the determination of covalent bond strength in ssDNA or dsDNA, it is also possible to evaluate the strength of the bonds between complementary strands in a short dsDNA piece, or to determine the forces necessary to stretch an intact DNA molecule (Hansma et al., 1996). High-resolution AFM imaging can also be used to characterize the physical structure of a DNA helix (Fig. 2), and more complex DNA architectures and DNA – protein interactions can be visualized and characterized using atomic force microscopy. Yaneva et al., for example, confirmed that DNA-dependent protein kinase (DNA-PK) can bind to DNA without the assistance of Ku proteins, and that the latter shows a time-dependent preference for strand ends, by visualizing DNA-Ku and DNA-DNA-PK interactions using AFM (Yaneva et al., 1997). The affinity between cells and specific proteins can also be assessed by indenting the cell of interest with an AFM tip functionalized with the protein of interest (Han et al., 1995). Gaub et al. reported a method to distinguish between individual red blood cell origins in a mixture of A- and O-group erythrocytes, using an AFM tip functionalized with *Helix pomatia* lectin (Grandbois et al., 2000).

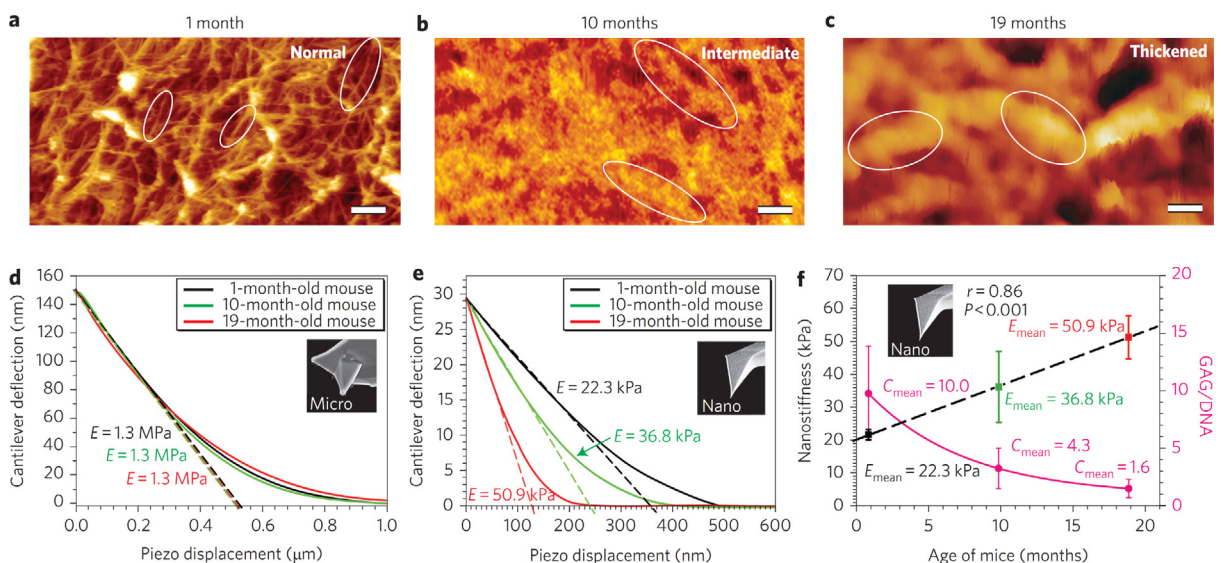


Fig. 1. Comparison of micro- and nanoindentation for the identification of changes associated with aging in the cartilage of C57BL/6 mice. Microindentation results could detect no difference between 1, 10 and 19-month old individuals, while nanoindentation was able to determine that the cartilage elasticity of non-arthritic mice changes with age. Replicated with permission from Stoltz et al. (2009b).

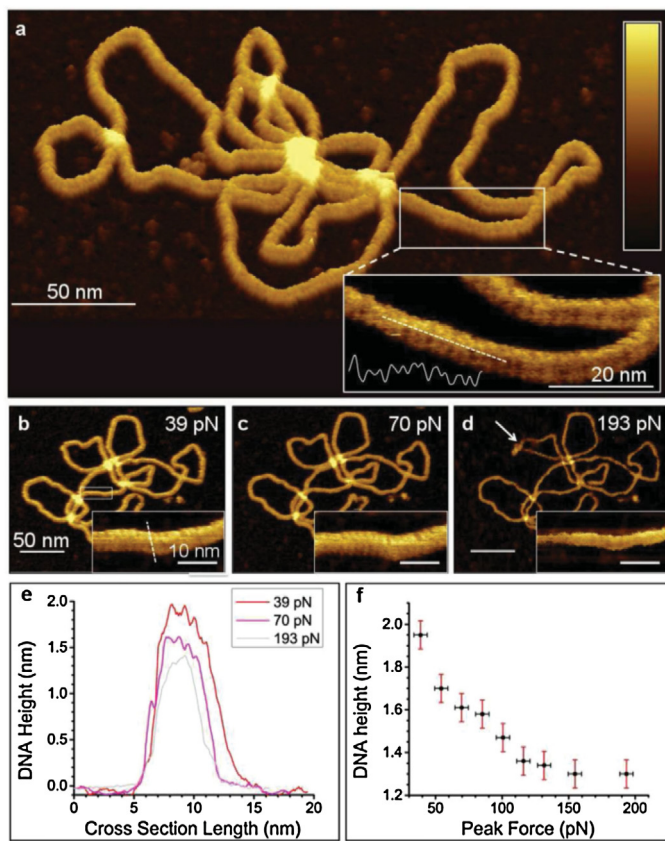


Fig. 2. AFM topography of a plasmid, showing the general appearance of the DNA helix under varying peak forces (a-d). Minor and major grooves can be observed in AFM images (a-d, insets), and the DNA structure can be compressed under high peak forces (e, f). White arrow denotes a dislocation in a plasmid loop created by high load forces. Replicated with permission from Pyne et al. (2014).

This lectin displays strong affinity to glycolipids that are present in the membranes of A-group but not O-group erythrocytes, resulting in higher rupture forces associated with the former. The differences

in adhesive forces are then utilized to create a map where individual A- and O-group cells can be identified.

3. Atomic force microscopy of unicellular organisms

A representative selection of AFM studies on the stiffness characterization of bacteria, yeasts and cellular secretions is provided in Table 1. It is readily evident that several means of sample preparation are available for measurement, and that values such as tip-sample adhesion, F-d curve slopes and cellular spring constants can all be used to compare the mechanical integrities of biological samples; consequently, only these studies detailing the full range of measurement conditions were included into the table. Both air and liquid imaging have been performed for mechanical investigations; however, biological materials are often viscoelastic and may display large changes in elastic behavior depending on environmental humidity. As such, samples in air tend to have much larger Young's moduli compared to samples imaged in liquids (e.g. a 10-fold difference was observed in between the elastic moduli of air-dried and rehydrated murine sacculi from *Escherichia coli* (Yao et al., 1999)). Given the differences in measurement techniques and sample preparation methods, as well as the natural variance in the material properties of bacterial cells and their secretions, it is usually preferable to compare results within studies rather than assuming a given stiffness value will apply under other experimental conditions.

3.1. Bacterial cell surfaces

Unlike many vertebrate cell lines, bacterial cells are not dependent on a highly specific set of environmental conditions to survive, and can tolerate extended AFM imaging sessions without detrimental effects (Raman et al., 2011; Francius et al., 2008). Their ease of procurement, non-demanding growth conditions and the fact that many laboratory species either are, or serve as models for, common pathogens make bacteria popular targets for AFM imaging. Bacteria must be immobilized prior to imaging in liquid media, as their mobility otherwise makes it impossible to image, and even sessile bacteria can be laterally pushed by the AFM tip (Doktycz et al., 2003). Immobilization can be performed by drying and rehydrating, electrostatic binding to a positively charged surface (e.g. gelatin or

Table 1
Mechanical characterization of membranes, secretions and single-celled organisms by AFM.

Sample	Tip properties	Imaging conditions	Elastic properties	Reference
Sulfate-reducing bacteria	Silicon nitride, $k = 0.06 \text{ N/m}$ (nominal)	Contact mode, air, sample on mica	(Adhesion) $-3.9 \text{ to } -4.3 \text{ nN}$ at cell surface, $-5.1 \text{ to } -5.9 \text{ nN}$ at cell-substrate boundary, $-6.5 \text{ to } -6.8 \text{ nN}$ at cell-cell boundary (F-d slope) 0.133 for wild-type strain on agar, 0.069 for wild-type strain in broth, 0.81 for dispersin mutant on agar, 0.78 for dispersin mutant in broth	Fang et al. (2000)
Enteropathogenic <i>Escherichia coli</i> , wild-type and dispersin mutant	Silicon, $k = 2.8 \text{ N/m}$ (nominal)	Contact mode, liquid (distilled water) and air, sample on gelatin-treated mica		Beckmann et al. (2006)
<i>Bacillus subtilis</i> , <i>Micrococcus luteus</i> , <i>Pseudomonas putida</i> , two strains of <i>Escherichia coli</i>	Silicon nitride, $k = 0.32 \text{ N/m}$ (nominal)	Contact mode, liquid (HM buffer), sample on APTES coverslip	(Spring constant) varies between 0.16 ± 0.01 to 0.41 ± 0.01 , higher in Gram-positive cells	Volle et al. (2008)
<i>Pseudomonas aeruginosa</i>	Silicon nitride and silicon nitride with silicon oxide tips, $k = 0.07 \pm 0.01$ (calibrated by the thermal method)	Contact mode, liquid (milliQ water), sample on poly-L-lysine-coated glass	(Spring constant) $0.044 \pm 0.002 \text{ N/m}$ for unfixed, $0.11 \pm 0.03 \text{ N/m}$ for glutaraldehyde-fixed cells; creep deformation behavior also investigated (Adhesion) $-0.26 \pm 0.05 \text{ nN}$ for membrane filter, -0.5 ± 0.2 for poly-L-lysine, $-35 \pm 2 \text{ nN}$ for glutaraldehyde fixation, other adhesion parameters also measured	Vadillo-Rodriguez et al. (2008)
<i>Klebsiella terrigena</i>	Silicon nitride, $k = 0.06 \text{ N/m}$ (nominal)	Contact mode, liquid (potassium phosphate buffer at pH 6.8), sample on polycarbonate membrane filter/poly-L-lysine-coated glass/immobilized on tip by gluteraldehyde fixation		Vadillo-Rodrigues et al. (2004)
Two <i>Streptococcus salivarius</i> strains	Silicon nitride, $k = 0.03 \text{ N/m}$ (nominal)	Contact mode, liquid (deionized water or 0.1 M KCl solution), sample on polycarbonate membrane filter	(Adhesion and repulsion) Fibrillated strain shows a larger repulsion range, interpreted to reflect the layer of fibrils; retraction results in three adhesion forces potentially corresponding to three different lengths of fibrils observed by electron microscopy (Adhesion) All three isolates adhere to aluminum better than mild steel, stainless steel 316 and copper; <i>Desulfovibrio</i> and <i>Pseudomonas</i> adhere better than the marine isolate.	van der Mei et al. (2000)
<i>Desulfovibrio desulfuricans</i> , <i>Pseudomonas</i> sp. and an unidentified local marine isolate	Silicon nitride, $k = 0.12 \pm 0.02 \text{ N/m}$ (calibrated by the thermal method)	Contact mode, liquid (artificial seawater), sample coated on tip and brought into interaction with metals		Sheng et al. (2007)
<i>B. mycoides</i>	Silicon, $k = 0.064 \text{ N/m}$ and 0.4 N/m	Contact mode (constant height), liquid (0.145 M NaCl), sample coated on tip and brought into interaction with glass	(Adhesion) $7.4 \pm 3.7 \text{ nN}$ of adhesion to hydrophilic glass surface, $49.5 \pm 14.42 \text{ nN}$ of adhesion to hydrophobic-coated glass surface	Bowen et al. (2002)
Marine bacterial depositions	Silicon, $k = 45.7 \text{ N/m}$ (calibrated by the added mass method)	Tapping mode, air, sample deposited on fluoridated and non-fluoridated polyurethane	(Young's modulus) between 1.5 and 2.2 GPa	Bakker et al. (2003)
Bacterial depositions, suspected to be extracellular polymeric substances	Silicon nitride, k varies from 0.03 to 0.5 N/m (nominal)	Contact mode, liquid (MilliQ water), sample deposited on polystyrene	(Adhesion) Forces of $0.8 \pm 0.2 \text{ nN}$ observed over bare polystyrene, as opposed to $0.2 \pm 0.2 \text{ nN}$ after cell attachment	van der Aa and Dufrene (2002)
<i>P. aeruginosa</i> pili	Silicon nitride, $0.008 \pm 0.004 \text{ N/m}$	Contact mode, liquid (water), sample attached to poly-L-lysine-coated tips and brought into interaction with mica surface	(Adhesion) Rupture forces of 95 pN during retraction.	Touhami et al. (2006)
<i>E. coli</i> biofilms	Silicon nitride, $k = 0.07\text{--}0.4 \text{ N/m}$	Contact mode, air, sample deposited on glass	(Adhesion) Pull-off forces of 122.65 pN for cell-tip interaction and 51.79 pN for glass-tip interaction	Oh et al. (2007)
Bacterial cellulose fibers	Silicon nitride $k = 1.03 \pm 0.05 \text{ N/m}$ (calibrated by the thermal method, nominal k of 0.5 N/m not used due to large discrepancy)	Contact mode, air, sample on silicon nitride-coated silicon grating	(Young's modulus) $78 \pm 17 \text{ GPa}$	Guhados et al. (2005)
<i>E. coli</i> and <i>E. coli</i> spheroplasts	Silicon nitride, $k = 0.1$ and 0.01 N/m (nominal, actual spring constants calibrated by the thermal method)	Contact mode, liquid (TBS2 buffer), sample on APTES/Glut mica	(Spring constant) 0.194 N/m for intact cells, 0.571 N/m for fixed spheroplasts	Sullivan et al. (2007)
<i>Saccharomyces cerevisiae</i>	Silicon nitride, $k = 0.008 \pm 0.4 \text{ N/m}$ (calibrated by the thermal method)	Contact mode, liquid (milliQ water), sample on polycarbonate membrane filter	(Young's modulus) $6.1 \pm 2.4 \text{ MPa}$ on bud scar, $0.6 \pm 0.4 \text{ MPa}$ on surrounding cell wall	Touhami et al. (2003)
<i>Aspergillus nidulans</i>	Silicon nitride, $k = 0.47 \pm 0.06 \text{ N/m}$ (calibrated by the thermal method)	Contact mode, liquid (PBS), sample on poly-L-lysine-coated glass	(Spring constant and Young's modulus) $0.29 \pm 0.02 \text{ N/m}$ and $110 \pm 10 \text{ MPa}$ for wild-type hyphae in complete medium, decreases for mutant strain lacking a chitin synthesis gene, as well as in the presence of 0.6 M KCl.	Zhao et al. (2005)

poly-L-lysine), entrapment in adhesive proteins, covalent binding to amino- or carboxyl-functionalized surfaces or by physical confinement in microwells or porous membranes (Doktycz et al., 2003; Suo et al., 2008). It should be kept in mind that the immobilization method may alter the surface properties of the entrapped cells, e.g. by directly altering the bacterial surface chemistry or triggering a defense mechanism against the environmental stresses associated with the immobilization technique. Due to the small sizes of bacteria, it is also possible to functionalize AFM tips with bacterial cells, which can then be used to test the interaction between the bacterium and material surfaces. Ting et al., for example, used such tips to show that the Gram-negative bacteria *Massilia timonae* and *Pseudomonas aeruginosa* adhere better to stainless steel surfaces than does the Gram-positive *Bacillus subtilis* (Harimawan et al., 2011).

AFM studies of bacteria frequently focus on the mechanisms by which certain molecules inhibit the growth of pathogens. Many antibiotics (e.g. beta-lactam antibiotics, polymyxins and glycopeptide antibiotics) act by inhibiting the synthesis of bacterial cell walls or membranes, and thereby alter the membrane integrity of the affected bacteria. Other antibiotic-mediated effects, such as membrane thinning (Mecke et al., 2005) or pore formation (Muller et al., 1999), can also be observed by AFM, and the effects of less conventional antibiotics, such as plant extracts (Perry et al., 2009) and peptide sequences (da Silva and Teschke, 2005; Meincken et al., 2005), can also be assessed (Fig. 3). The antimicrobial peptide PGLa has been demonstrated to lower the stiffness of *Escherichia coli* membranes and create micelle-like structures around cell membranes prior to their eventual rupture, while garlic extract was also associated with membrane disruption. Chitosan and chitooligosaccharides (COSSs) were also tested for their antimicrobial effect on *E. coli* and *Staphylococcus aureus*, and the thick peptidoglycan wall of *S. aureus* was found to allow this bacterium to better retain its overall morphology, despite experiencing a significant decrease in cell rigidity (Fernandes et al., 2009). While the effects of antibacterial molecules may be apparent even under dry imaging, it is also possible to quantify the resulting changes in a time-dependent manner by characterizing the mechanical properties of bacterial cells in liquid before and after introducing the antibiotic in question into the medium (Fantner et al., 2010a). This technique has the advantage of ensuring that the changes observed are fully due to the antibiotic, as opposed to a combination of it and the drying process, as bacterial cell walls are viscoelastic and may greatly alter their mechanical properties in response to relative humidity (Thwaites and Surana, 1991).

A variety of subcellular elements can also be identified on membrane surfaces using AFM. Both bacterial and eukaryotic cells can be used in these efforts, and lipid bilayers can be substituted as simplified models of cell membranes (Butt et al., 1990; Kuznetsov and McPherson, 2011). The structure and function of membrane proteins (Butt et al., 1990; Fotiadis et al., 2003; Yuan et al., 2002), pore complexes (Stoffler et al., 1999), gap junctions (Lal and John, 1994), amyloid aggregates (Connelly et al., 2012) and a variety of membrane-component lipids (Györvary et al., 2003a), as well as the mode of action of cholera toxin (Mou et al., 1995), were investigated by atomic force microscopy. Of particular interest are the recent developments in AFM-based rapid, high-resolution imaging methods, which have granted substantial insight into the nature of small surface elements. Processes such as the self-assembly of bacterial S-layer proteins (Györvary et al., 2003b), protein folding (Muller et al., 2002), misfolding (Oberhauser et al., 1999) and crystallization (Reviakine et al., 1998) events, the motion of "walking" proteins (Preiner et al., 2014) and drug-membrane interactions (Berquand et al., 2004) have been the subject of real-time imaging studies.

3.2. Bacterial secretions, exudates and biofilms

It is well-known that cells in multicellular organisms enhance their survival and coordination through the production of an extracellular matrix; however, this property is not unique to higher eukaryotes. Bacteria also secrete proteins, polysaccharides and quorum sensing molecules that relay information between conspecific cells and serve as a buffer against environmental stresses. In addition, the surface attachment of bacteria is also mediated by extracellular depositions, the adhesion capacities of which can be measured through AFM. Colanic acid production and surface lipopolysaccharide lengths, for example, were previously demonstrated to determine the strength of attachment of *E. coli* cells, as colanic acid-overproducing mutants were found to exhibit stronger attachment while shorter surface lipopolysaccharides were associated with a lack of adhesive capacity (Razatos et al., 1998).

Bacterial biofilms are also of special interest with regards to AFM characterization. Biofilms are extracellular polysaccharides that are secreted to facilitate the attachment of bacteria (or other unicellular organisms) to a surface, and protect the adhering cells against hostile environmental factors such as antibiotics, detergents and heavy metals (Davies et al., 1998). Biofilms are undesirable elements in many settings, and suitable means to inhibit their formation is necessary to prevent potential health hazards in food, agricultural and medical industries. As such, the mechanical properties of biofilms, as well as the mechanisms by which antifouling molecules act against biofilm production, have been investigated by using AFM and other mechanical characterization techniques (Beech et al., 2002; Arnold and Bailey, 2000). Corrosion damage and adhesive capacity of biofilms on a variety of metal surfaces have been detailed in the literature: Holden et al. report that unsaturated and liquid-grown biofilms of *Pseudomonas putida* respond differently to drying, suggesting that the biofilm composition is altered for optimal growth in dry and wet environments (Auerbach et al., 2000). In another report, Tay et al. detail the effect of silver ions on *Staphylococcus epidermidis* biofilms and propose a mechanism through which silver destabilizes the biofilm structure by binding to the electron donor groups provided by the biofilm components, thereby weakening the hydrogen bonds that hold the biofilm matrix together (Chaw et al., 2005).

4. Atomic force microscopy of mammalian cells and tissues

A selection of AFM studies on the stiffness characterization of eukaryotic cells and tissues is provided in Table 2. AFM of mammalian cells and tissues is often undertaken for disease diagnosis or stem cell differentiation studies, as diseased tissues often display mechanical characteristics distinct from their healthy counterparts and stem cells are widely known to alter their differentiation pathways and mechanical characteristics depending on external stimuli. Consequently, AFM of cancer and stem cells can provide greater insight into the pathways required for events such as metastasis and lineage commitment. However, measurement of these samples is more difficult than single-cellular organisms or non-living biological materials such as biofilms and other secretions, as mammalian cells require a specific set of environmental conditions to survive and environmental stress can have a major impact on their mechanical properties. In addition, while fixative treatment can be used prior to imaging, fixation may greatly alter the mechanical properties of eukaryotic cells, and live cell imaging is generally required to acquire reliable elasticity data (Fig. 4). Nonetheless, cell culture conditions can be replicated to some extent within the liquid cell of an AFM, and a large number of successful investigations have been made regarding the mechanical character of living

Table 2
Mechanical characterization of mammalian cells and tissues by AFM.

Sample	Tip properties	Imaging conditions	Elastic properties	Reference
NIH3T3 fibroblasts	Silicon nitride, $k = 0.018 \text{ N/m}$ (calibrated by thermal method)	Contact mode, liquid (DMEM containing D-glucose (1000 mg/L) and 10% fetal bovine serum, fresh, warmed Ringer's solution used as medium replenishment), sample on fibronectin-coated glass	(Young's modulus) 4–100 kPa over the cell surface, lower around the nucleus than in the periphery	Haga et al. (2000)
Breast cancer lines (MCF-10A and MCF7)	Silicon nitride, $k = 0.01 \text{ N/m}$ (nominal) modified with a 4.5 μm diameter polystyrene bead	Contact mode, liquid (culture medium), sample on glass	(Young's modulus) 0.2–1.2 kPa range, malignant cell line (MCF7) 1.4–1.8 times softer than benign cell line (MCF-10A)	Li et al. (2008)
Osteoblasts, mesenchymal stem cells and osteosarcoma cells	Silicon nitride, $k \sim 20 \text{ N/m}$ (calibrated using thermal method)	Contact mode, liquid (25 mM HEPES), fixed cells on polystyrene, glass or collagen-coated glass	(Young's modulus) 0.7 ± 0.1 to $2.6 \pm 0.7 \text{ kPa}$ range, lower Young's modulus for MG63 osteosarcoma cells on collagen	Docheva et al. (2008)
Zonal articular chondrocytes	Spherical gold-coated borosilicate bead (5 μm diameter), $k \sim 0.065 \text{ N/m}$ (calibrated by thermal method)	Contact mode, liquid (DMEM), sample on poly-L-lysine-coated glass	(Young's modulus) Instantaneous moduli at $0.55 \pm 0.23 \text{ kPa}$ for superficial, $0.29 \pm 0.14 \text{ kPa}$ for middle/deep cells; relaxed moduli at $0.31 \pm 0.15 \text{ kPa}$ for superficial, $0.17 \pm 0.09 \text{ kPa}$ for middle/deep cells; apparent viscosities at $1.15 \pm 0.66 \text{ kPa s}$ for superficial, $0.61 \pm 0.69 \text{ kPa s}$ for middle/deep cells	Darling et al. (2006)
Cardiac muscle, skeletal muscle and endothelial cells	Silicon nitride, $k = 0.03$ to 0.05 N/m (calibrated using thermal method)	Contact mode, liquid (growth medium), sample on glass slide	(Young's modulus) Moduli of $100.3 \pm 10.7 \text{ kPa}$ for cardiac muscle, $24.7 \pm 3.5 \text{ kPa}$ for skeletal muscle and 1.4 ± 0.1 to $6.8 \pm 0.4 \text{ kPa}$ depending on the region tested for epithelial cells	Mathur et al. (2001)
Cardiac myocytes	Silicon nitride, $k = 0.06 \text{ N/m}$ (nominal)	Contact mode, liquid (culture medium), sample on laminin-coated petri dish	(Young's modulus) $35.1 \pm 0.7 \text{ kPa}$ for cardiomyocytes from 4-month old rats, $42.5 \pm 1.0 \text{ kPa}$ for cardiomyocytes from 30-month old rats.	Lieber et al., (2004a)
LLC-PK1 and MDCK kidney epithelial cell lines	Silicon nitride, $k = 0.12 \text{ N/m}$ (nominal)	Contact mode, liquid (artificial urine)	(Young's modulus) $1.5 \pm 0.8 \text{ MPa}$ for LLC-PK1 cells, $5 \pm 1.5 \text{ MPa}$ for MDCK cells, oxalate treatment decreases Young's modulus to $1.2 \pm \text{MPa}$ for LLC-PK1 cells (other stiffness parameters also measured) (Young's modulus) 3–7 kPa for the C domain, 7–23 kPa for the T domain, 10–40 kPa for the P domain	Rabinovich et al. (2005)
Neuronal growth cones	Silicon nitride, $k = 0.006 \text{ N/m}$ (nominal)	Contact and dynamic modes, liquid (L15/ASW medium), sample on poly-L-lysine-coated glass	(Young's modulus) 3–7 kPa for the C domain, 7–23 kPa for the T domain, 10–40 kPa for the P domain	Xiong et al. (2009)
Healthy and pathological erythrocytes	Silicon nitride, $k = 0.03$ (nominal)	Contact, liquid (PBS), sample on poly-L-lysine-coated glass and fixed by glutaraldehyde	(Young's modulus) Moduli of $26 \pm 7 \text{ kPa}$ for healthy erythrocytes, $43 \pm 21 \text{ kPa}$ for hereditary spherocytosis, $40 \pm 24 \text{ kPa}$ for thalassemia and $90 \pm 20 \text{ kPa}$ for G6PD deficiency samples	Dulinska et al. (2006)
Liver endothelial cells	Silicon nitride, $k = 0.032 \text{ N/m}$	Contact, liquid (serum-free endothelial cell medium), cells on collagen-coated petri dishes with and without glutaraldehyde fixation	(Young's modulus) Moduli of 2 kPa for living cells and over 100 kPa for fixed cells	Braet et al. (1998)
Oral squamous cell carcinoma, normal and malignant lines	Silicon nitride tip, $k = 0.01$ to 0.1 N/m ; APTES-modified silicon oxide sphere tip, $k \sim 0.5 \text{ N/m}$ (calibrated using Sader method)	Contact, air, sample pre-fixed with 2% PFA and fixed with 3.7% PFA	(Young's modulus) Median values of 6.75 MPa for "normal" and 4.36 MPa for metastatic cancer cells. Elasticity measurements taken using sphere-modified tips.	Lasalvia et al. (2015)
PC-3 prostate cancer cells	Silicon nitride tip, $k = 0.012 \text{ N/m}$ (calibrated using thermal method)	Contact, liquid (culture medium), samples treated with anticancer drugs or DMSO control for 24 h prior to analysis	(Young's modulus) c. 3 kPa for untreated cells, increased to c. 6–12 kPa in a dose-dependent manner following drug treatment. Frequency-dependency of the elastic modulus was also tested and found to change significantly for Celebrex, BAY, Totamine, TPA and VPA treatment, but not for DSF, MK and Taxol. This effect is linked to the fact that the former drugs may alter crosslinking rates of cytoskeletal filaments, while the latter only change fiber length and thickness.	Ren et al. (2015)

Table 2 (Continued)

Sample	Tip properties	Imaging conditions	Elastic properties	Reference
Normal and cancerous bladder epithelium cells	Silicon nitride tip, $k = 0.011$ to 0.018 (calibrated using thermal method)	Contact, liquid (culture medium), sample on glass	(Adhesion energy) average of 8.17×10^{-16} J for normal, 26.95×10^{-16} J for cancer cells (Young's modulus) average of 27.57 kPa for normal, 2.46 kPa for cancer cells	Canetta et al. (2014)
Porcine articular cartilage	Silicon nitride, $k = 0.06$ N/m (nominal) and borosilicate glass beads with $r = 2.5$ μm , $k = 0.06$ and 13 N/m (nominal)	Contact, liquid (PBS), tissues on poly-L-lysine-coated glass	(Dynamic elastic modulus) On the order of 2.6 MPa for borosilicate glass beads, about 100-fold lower for sharp tips	Stolz et al. (2004)
Articular cartilage of normal and arthritic (<i>Col9a1</i> ^{-/-} knockout) mice	Silicon nitride, $k = 0.06$ N/m (nominal) and microspheres, $k = 10$ and 12 N/m	Contact, liquid (PBS), bulk tissues glued on a round Teflon disk	(Dynamic elastic modulus) 1.3 ± 0.4 MPa for microspheres (no change recorded between ages); 22.3 ± 1.5 kPa, 36.8 ± 1.5 kPa and 50.9 ± 4.7 kPa for sharp tips in 1-, 10- and 19-month old normal mice; 22.3 ± 1.5 kPa, 25.5 ± 1 kPa and 27.7 ± 1.1 kPa in the non-thickened, intermediate and heavily thickened collagen fibers of 1-month old arthritic mice. (Young's modulus) 0.4 – 0.5 MPa range for blood vessels without drug influence, raised to c. 1.0 MPa in the presence of nitroglycerin and decreased back to c. 0.3 MPa in the presence of norepinephrine	Stolz et al. (2009b)
Aortic intima of rats	Not listed, tip mounted on a custom platform for <i>in vivo</i> AFM imaging	Anaesthetized living animals		Mao et al. (2009)
Anterior human corneal stroma	Phosphorus-doped silicon, $k = 25$ and 33 N/m (calibrated by an optical method, as described by Sader et al.)	Contact, liquid (15% dextran), bulk tissue placed on Teflon cell without attachment	(Young's modulus) Between 1.14 and 2.63 MPa, consistent across the indentation depths (between 1.0 and 2.7 μm)	Lombardo et al. (2012), Sader et al. (1999)
Human corneal basement membrane	Borosilicate glass, $k = 0.06$ N/m (nominal)	Contact, liquid (PBS), a 3×3 mm tissue piece dissected and glued onto a well on steel disk	(Young's modulus) 2 – 15 kPa, mean of 7.5 ± 4.2 kPa average for the anterior basement membrane; 20 – 80 kPa, 50 ± 17.8 kPa average for the Descemet's membrane	Last et al. (2009)
Monkey lenses	Gold-coated tip, $k = 0.01$ N/m (nominal), calibrated by the relationship between applied voltage and cantilever deflection	Contact, liquid (BSS), lenses dissected and placed on Teflon slide	(Young's modulus) 1.720 ± 0.88 kPa	Ziebarth et al. (2007)
Human bone	Various	Various	(Young's modulus) 16.6 ± 1.1 to 27.1 ± 1.7 for dry adult tibiae (lower for children), 13.4 ± 2.0 to 22.7 ± 3.1 for dry adult vertebrae (lower for wet samples), 16.58 ± 0.32 to 26.6 ± 2.1 for dry adult femoral midshaft (lower for wet samples and in the femoral neck), other bone measurements and tissue hardnesses also noted (Young's modulus) 60 ± 2.69 MPa for lateral rectus, 59.69 ± 5.34 MPa for inferior rectus, 56.92 ± 1.91 MPa for medial rectus, 59.66 ± 2.64 MPa for superior rectus, 57.7 ± 1.36 MPa for inferior oblique and 59.15 ± 2.03 for superior oblique tendons. Differences between tendon elasticities are not statistically significant.	Thurner (2009)
Bovine ocular tendon fibers	Silicon nitride tip, $k = 0.02$ N/m (calibrated using thermal method)	Contact, air (sampling chamber kept at 100% humidity), sample glued on glass petri dish	(Young's modulus) 60 ± 2.69 MPa for lateral rectus, 59.69 ± 5.34 MPa for inferior rectus, 56.92 ± 1.91 MPa for medial rectus, 59.66 ± 2.64 MPa for superior rectus, 57.7 ± 1.36 MPa for inferior oblique and 59.15 ± 2.03 for superior oblique tendons. Differences between tendon elasticities are not statistically significant.	Yoo et al. (2014)
Breast tissue sections	Borosilicate glass tip, $k = 0.06$ N/m (nominal), individual tips calibrated using thermal method	Contact, liquid (PBS supplied with protease inhibitors and propidium iodide), samples sectioned by cryomicrotomy	(Young's modulus) c. 400 P in healthy and non-invasive tumor regions, 4-fold increase in average stiffness in invasive tumor front. Higher average stiffness in the invasive front is caused by highly stiff (> 5 kPa) regions in this area. Aggressive breast cancer subtypes are also found to exhibit higher Young's moduli, quantified in terms of upper 10% stiffness.	Acerbi et al. (2015)
Benign and aggressive prostate tumors	Silicon nitride tip, $k = 0.06$ N/m (nominal), individual tips calibrated using thermal method	Contact, liquid (physiological buffer), sample sliced by razor and glued on glass	(Young's modulus) 3.03 ± 0.64 kPa for benign, 1.72 ± 1.22 for cancerous tissues. The average Young's modulus for cancer samples with Gleason scores in the 2–7 range was 2.07 ± 1.30 , this value was 1.39 ± 0.48 for samples with Gleason scores in the 8–10 range. In addition, metastatic tumors had an average modulus of 1.06 ± 0.58 , while non-metastatic cancer tissue had an average elasticity value of 1.99 ± 1.24 . These values reflect the tissue microenvironment and contrast macro-scale elastography results, in which more aggressive cancers are stiffer.	Wang et al. (2014)

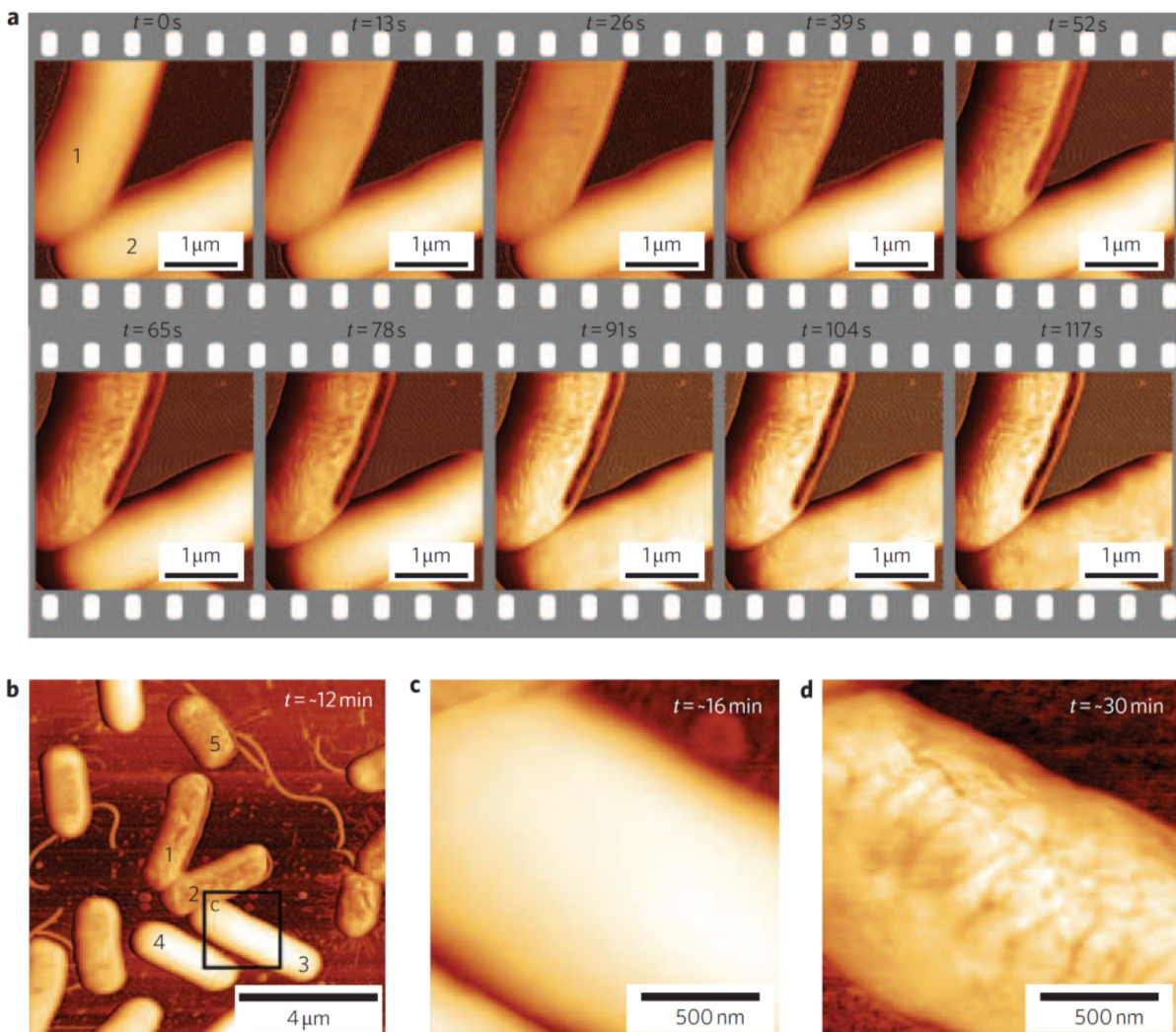


Fig. 3. The effect of an antimicrobial peptide (CM15) on *E. coli* cell walls, as observed by high-speed AFM. Disruptions begin to appear on cell surfaces as early as $t = 13\text{ s}$ and increase in severity with time (a). Although some bacteria resist the effects of the peptide (b, c), these individuals nevertheless react to prolonged treatment (d, at $t = \sim 30\text{ min}$). Replicated with permission from Fantner et al. (2010b).

mammalian cells and tissues, either cultured *ex vivo* or collected immediately prior to imaging.

4.1. Cancer diagnosis and characterization

While medical advances have led to significant decreases in the incidences of many cancers, cancer still remains to be one of the most important diseases in recent history. It is well-established that cancer cells exhibit marked differences in stiffness and elasticity compared to their healthy counterparts (Cross et al., 2007); however, diagnostic applications of mechanical characterization methods should currently be considered limited. Effective diagnostic techniques must ascertain the presence (or absence) of disease with high confidence and using minimal amounts of sample tissue and time, and despite the ability of mechanical measurements to effectively distinguish between healthy and tumor cells, it is unlikely that a biopsy at an early stage of disease would yield tumor cells in numbers necessary to perform diagnosis based purely on mechanical data. Nonetheless, once the presence of a tumor is confirmed using more conventional methods, AFM may serve as a valuable tool for its characterization: Laidler et al., for example, report the possibility of utilizing AFM to determine whether a suspected breast or prostate tumor is malignant on the basis of its

elastic properties (Lekka et al., 2012). In addition, AFM cantilevers can be functionalized with antibodies for disease-specific markers and used in the detection of cancer and other disorders (Laurent et al., 2014); however, this technique effectively converts the AFM into a biosensor or sorting system instead of relying on its capacity for mechanical characterization.

Greater utility lies in the characterization of tumor cells and their interactions by AFM, which may further the current understanding of cancer biology and allow the design and evaluation of novel cancer drugs. Discrepancies between the elasticities of cancer and non-malignant cells, for example, have been recorded in human lung, breast, pancreas, fibroblast, prostate, adenocarcinoma and other cell lines (Muller and Dufrene, 2008; Cross et al., 2011). These changes are suspected to increase the mobility of malignant cells during metastasis, and decreases in cell stiffness appear to be progressive, with more malignant cells expressing lower Young's moduli. Fuhrmann et al. reported that the dysplastic Barrett's esophagus cell lines are less rigid compared to metaplastic cells, which in turn are softer than their healthy counterparts (Fuhrmann et al., 2011). Other changes in cell morphology may also occur to facilitate metastasis, and these too can be quantified by AFM. Sokolov et al., for example, have determined that cancerous human cervical epithelial cells display two brush layers,

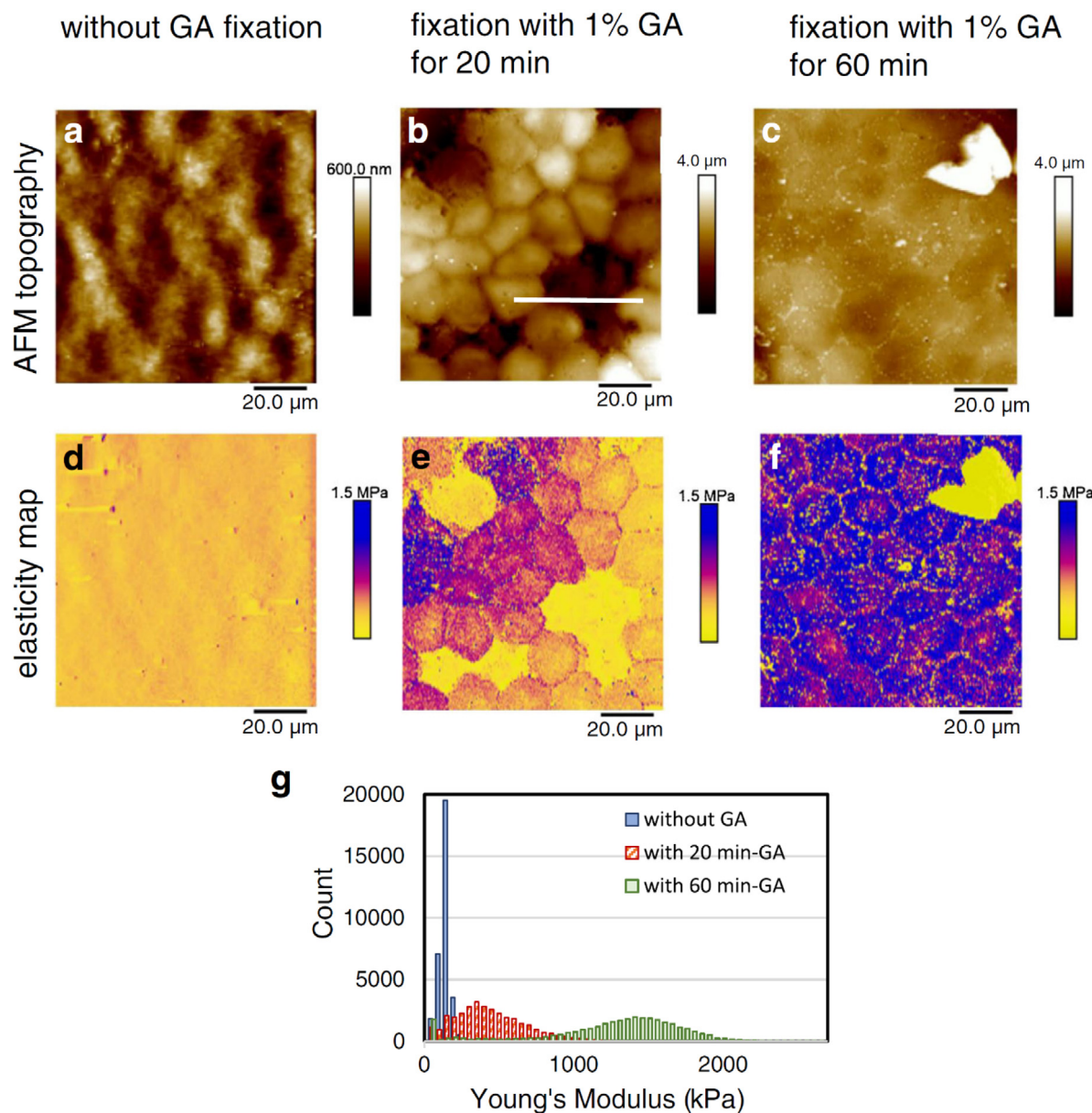


Fig. 4. Effect of fixation on cellular elasticity. Unfixed (a, d) and GA-fixed (b and e for 20 min; c and f for 60 min) cells have distinct appearances and elastic moduli; with GA fixation greatly increasing cellular Young's moduli in a time-dependent manner (g). Replicated with permission from [Shibata-Seki et al. \(2015\)](#).

in contrast to the single-length molecular brush of non-malignant cervical epithelium, which may also assist in invasion attempts by these malignant cells ([Iyer et al., 2009](#)). In addition, the tumor microenvironment also appears to contribute significantly to the alterations in tumor elasticity: Instead of the expected decrease in Young's moduli, Weaver et al. observed a time-dependent increase in tumor stiffness during mammary tumor development in PyMT mice, and this increase in rigidity was also reflected in epithelial cells taken from the tumor site. However, cells taken out of their native environment and grown *in vitro* had lower Young's moduli compared to their *in vivo* counterparts, and the inhibition of the ECM-crosslinking enzyme lysyl oxidase mitigated the gradual increase in the elastic modulus of mammary gland tumors ([Fig. 5](#)) ([Lopez et al., 2011](#)). As such, tissue culture samples and *in vivo* tumor cells may not necessarily agree in elastic properties, as the stiffness of the former depends on the cytoskeletal properties of the cells, while that of the latter is largely mediated by the tissue microenvironment.

Drug responses of cancer cells can also be quantified by AFM. Zhang et al. observed that HeLa, HepG2 and C6 cells experience dose-dependent morphological changes on their cell membranes following treatment with colchicine or cytarabine. Surface roughness increased and pores appeared on the cell membrane after drug administration and before MTT-quantifiable decreases in viability could be observed, suggesting that the surface alterations represent an early response to drug presence ([Wang et al., 2009](#)). Such differences may be monitored to evaluate the effectiveness of drug candidates. Changes associated with gene deletion or restoration can also be observed through AFM: Zhou et al. reported that the expression of BRMS1 (restoring breast cancer metastasis suppressor 1) induces increases in cell adhesion capacity, cellular spring constant and Young's modulus, which supports the idea that BRMS1 expression is associated with cytoskeletal rearrangements that are unfavorable for metastatic activity. Cell morphology and roughness were also altered following BRMS1 expression, possibly as a consequence of cytoskeletal modifications ([Wu et al., 2010](#)).

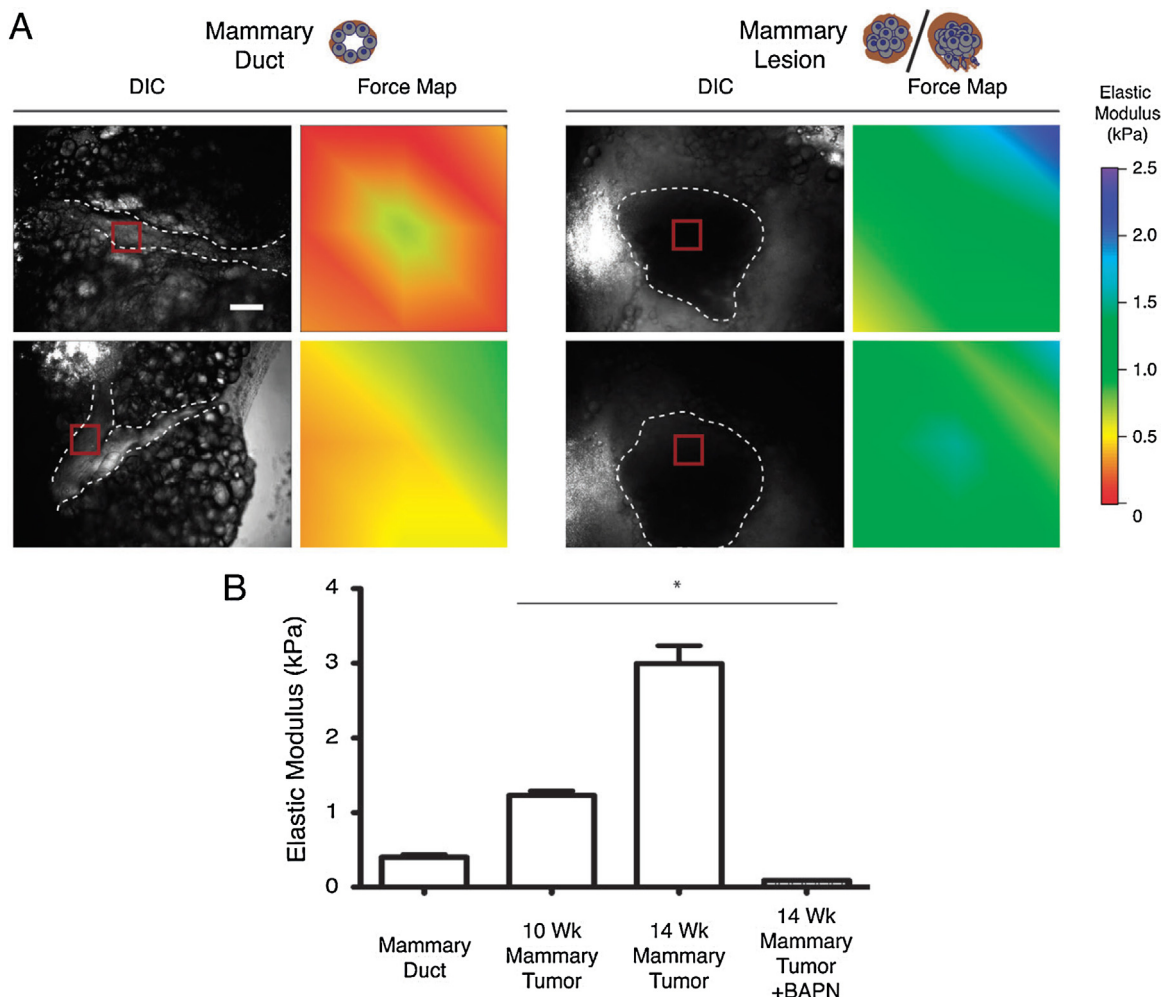


Fig. 5. Changes associated with mammary tumor formation, as quantified by AFM. Normal mammary duct tissue is less stiff compared to tumor tissue (a), and the tissue elastic modulus increases with tumor age (b). In addition, the inhibition of collagen cross-linking by BAPN (which blocks the activity of lysyl oxidase) prevents the tumor-associated increase in stiffness, suggesting that the tumor environment is modified through changes in the extracellular matrix. Replicated with permission from Lopez et al. (2011).

4.2. Diagnosis of other diseases

While cancer-associated changes in cell elasticity are particularly drastic, cancer is by no means the only condition to alter the mechanical properties of affected tissues. A variety of other conditions, including malaria, sickle cell anemia, hepatic fibrosis, cardiovascular disease, renal stiffness, muscular dystrophies and bone disorders, have also been associated with notable changes in the elastic properties of the affected tissues (Fig. 6) (Costa, 2003; Nagao et al., 2000; Lieber et al., 2004b; Bozec et al., 2005; Engler et al., 2004). Mechanical diagnosis methods have been devised for some such conditions, and AFM can be utilized to study the structural and mechanical properties of affected tissues; but it must be noted that, as with cancer, AFM-based diagnostic methods for these diseases currently appear to be more suited towards supporting conventional diagnosis. However, the high-resolution imaging and mechanical probing capacity of AFM is ideal for the determination of the causes underlying the progression of the diseases in question.

Several reports on AFM-based disease characterization exist in the literature. Szymoński et al., for example, demonstrate that red blood cells belonging to patients with hereditary blood diseases generally bear a higher Young's modulus compared to healthy erythrocytes (Dulinska et al., 2006). In particular, gluteraldehyde-fixed, poly-L-lysine-immobilized erythrocytes of patients with hereditary spherocytosis, thalassemia or G6PD deficiency were

stiffer compared to normal cells, while patients with anisocytosis displayed two distinct peaks in their histogram of Young's moduli, corresponding to healthy and diseased populations of cells. In patients with hereditary spherocytosis, changes in cell morphology were also observed. Similarly, Vatner et al. have investigated the effects of aging on cardiac myocytes by AFM indentation, comparing 4 month- and 30 month-old rats in order to assess whether myocyte health influences the aging-associated diastolic dysfunction of the left ventricle (Lieber et al., 2004b). Myocytes were found to significantly increase in stiffness with age, suggesting that the observed dysfunction can be linked at least in part to the malfunction of individual myocytes. The effect of aging on cellular Young's moduli was also noted by Sokolov et al., who have shown that older human epithelial cells are more rigid than their younger counterparts, and have further demonstrated that an increase in the density of cytoskeletal elements is responsible for the age-related increase in stiffness (Berdyyeva et al., 2005a,b). The early detection of osteoarthritis was also performed on the articular cartilage of normal and arthritic mice, and nanoindentation (but not micro-scale tips) was shown to resolve the gradual changes in cartilage stiffness between arthritic and non-arthritic animals of the same age (Stolz et al., 2009b).

Another interesting frontier in AFM-based disease characterization is the investigation of malfunctioning proteins that are involved in the pathogenesis of neurodegenerative disorders such

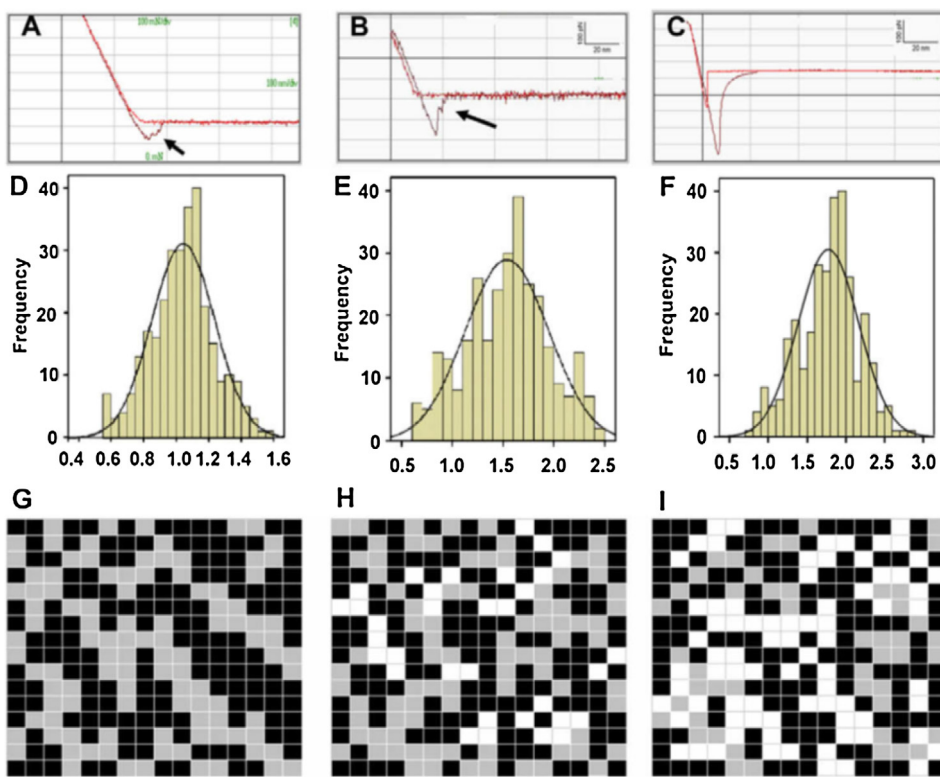


Fig. 6. Young's modulus measurements of erythrocytes from young and healthy (YHP; a, d and g); old and healthy (OHP; b, e and h) and old and type-II diabetic (ODP; c, f and i) individuals. Erythrocytes exhibited higher stiffness in ODP individuals compared to either YHP or OHP ($1.78 \pm 0.39 \times 10^5 \text{ N/m}^2$ v. $1.04 \pm 0.19 \times 10^5 \text{ N/m}^2$ and $1.53 \pm 0.41 \times 10^5 \text{ N/m}^2$, respectively). In addition, OHP and ODP erythrocytes exhibited higher adhesion compared to YHP erythrocytes ($420 \pm 25 \text{ pN}$ and $510 \pm 63 \text{ pN}$ v. $200 \pm 38 \text{ pN}$, respectively). Replicated with permission from Jin et al. (2010).

as Alzheimer's disease, Parkinson's disease, Huntington's disease and amyotrophic lateral sclerosis. These disorders severely decrease the quality of life, are exceptionally common among the elderly and have no definitive cures, which renders it crucial to gain further insight into the nature of their causative agents. As such, the formation of amyloid plaques has been investigated in detail using a variety of biological, chemical and material characterization methods, including several AFM-based studies. Lansbury et al., for example, reported on the *in vitro* formation of metastable A β amyloid fibril precursors that may later develop into complete amyloid assemblies, and suggest that the halting of this mechanism may prevent the onset of Alzheimer's disease by retaining the precursor fibrils ("protofibrils") in their benign intermediate form (Harper et al., 1997). In addition, Kowalewski and Holtzman demonstrated that the size, shape and production kinetics of A β aggregates were altered depending on the surface on which the aggregation occurs (Kowalewski and Holtzman, 1999) (*i.e.* particulate assemblies were generated on the hydrophilic mica surface, while β -sheets formed on the hydrophobic graphite), and suggested that the β -sheet forming behavior of A β on graphite may yield useful information on how protein folding occurs *in vivo*. The ability of A β peptides to form ion-channel like structures without interacting with other membrane components was also confirmed using AFM, with trimeric, tetrameric, pentameric and hexameric pore structures being identified in topographic images. Both D- and L-enantiomers of A β peptides were able to form these channels, suggesting that the pore formation mechanism is not stereospecific (Connelly et al., 2012).

4.3. Stem cell differentiation

Fluctuations in mechanical properties do not necessarily suggest aging-related deterioration or a disease state, as healthy cells may

also respond to environmental signals by altering their membrane integrity. This is most obviously observed in stem cells, as differentiation induces fundamental changes not only in cell morphology and expression patterns, but also in membrane content and stiffness (Discher, 2006; Evans et al., 2009; Reilly and Engler, 2010). Since the maintenance, recruitment and differentiation of stem cells are intimately linked to the mechanical properties of their immediate environment, it is feasible to use AFM measurements in order to determine the factors that drive the differentiation process in these cells. Such factors are relatively clear in some cases, such as the mesenchymal stem cell differentiation into myogenic, chondrogenic or osteogenic lineages, but the mechanical triggers behind the differentiation of other cells are well less understood. In addition to stem cell differentiation, changes in the microenvironmental conditions of tissues can be assessed using AFM or other mechanical characterization methods, especially in situations involving the slow recovery of a damaged system, as in the cases of bone fracture healing. Other processes, such as the local remodeling and extracellular matrix secretion of cells in a tissue culture environment, or the capacity of biomimetic materials to imitate the mechanical environment of their tissue model, also fall within the purview of AFM.

The differences between stem and derived cells have also been investigated by AFM. Guilak et al. have confirmed that chondrocytes, osteoblasts and adipocytes, the primary differentiation products of mesenchymal stem cells, display different rigidities, and determined that undifferentiated mesenchymal stem cells are similar to adipocytes in their mechanical characteristics (Darling et al., 2008). Schieker et al. reported that the two subcategories of human mesenchymal stem cells, flat cells and rapidly self-renewing cells, can also be differentiated on the basis of their morphological and adhesive characteristics (Docheva et al., 2008),

with the former type appearing topographically similar to human osteoblasts and displaying a high adhesion to the surface, while the latter exhibited characteristics similar to MG63 osteosarcoma cells and displayed a smoother topography. Even stem cell fate can be predicted by mechanical properties prior to the appearance of visible indicators. Gonzalez-Cruz and Darling reported that adipose-derived stem cells can be classified according to their differentiation potential to adipogenic, osteogenic or chondrogenic lineages on the basis of their mechanical behavior (Gonzalez-Cruz et al., 2012). As could be expected; softer, larger and more pliant adipose-derived stem cells are more likely to differentiate into adipocytes, while smaller and more rigid stem cells are inclined towards osteogenic or chondrogenic differentiation. In addition, the effect of stem cells on an *in vivo* environment can be determined following their implantation: Mesenchymal stem cells injected into the site of a myocardial infarction have been recorded to decrease the rigidity of the myocardium, which was associated with reduced fibrosis and a better prognosis for the postinfarcted heart.

The importance of the extracellular matrix (ECM) for the maintenance and differentiation of stem cells is both obvious and paramount (Bosnakovski et al., 2006; Suzuki et al., 2003). It is therefore unsurprising that the mechanical properties of ECM elements are vital in providing the signals responsible for inducing stem cells to differentiate, or for retaining them in their quiescent state (Reilly and Engler, 2010; Guilak et al., 2009). Great differences exist in the ECM rigidities of adult tissues, from 0.1 kPa in brain to >30 kPa in bone (Huang et al., 2012), and excessively soft or rigid tissues may result in suboptimal differentiation (see e.g. Engler et al. for an account of aberrant myotube formation associated with unsatisfactory surface stiffness (Engler et al., 2004)). In addition to adult stem cells in mature tissues, there is also evidence that *endo*-, *meso*- and ectodermal progenitors are arranged into distinctive germ layers with the assistance of differences in tensile strength (Discher et al., 2005; Puech et al., 2005): Cell-cortex tensions of endodermal progenitors in gastrulating zebrafish embryos are higher than that of the mesodermal progenitors, which in turn are larger than that of ectodermal progenitor cells (Fig. 7) (Krieg et al., 2008b). In a similar vein, cardiac looping in chicken embryos was suggested to occur as a result of a stiffness-mediated asymmetry in the developing cardiac jelly (Zamir et al., 2003).

4.4. Extracellular secretions and tissue microenvironments

AFM can be used to measure the native stiffness of tissue micro- and nanoenvironments, although other methods, such as microindentation, can also be used for the micromechanical investigation of larger areas of tissues. Bone, cartilage and the ocular tissues have been frequently investigated using AFM, and age- or disease-related effects have been found to be reflected in tissue stiffness. As with bacterial and eukaryotic cells, the method of sample preparation can greatly alter the elastic modulus of tissues, and sampling location likewise has a substantial effect on mechanical properties (Stolz et al., 2009b; Thurner, 2009). It must also be kept in mind that the micro- and nanoscale stiffnesses of a given tissue may differ greatly, e.g. the microstiffness of porcine articular cartilage was observed to be over 100-fold greater than its nanostiffness, and the age-related effects of osteoarthritis on the articular cartilage of mice could only be observed through nanoscale tips (Stolz et al., 2009a, 2004). As such, care must be taken not to compare the results of cell- or tissue-based AFM studies to literature examples that use dissimilar conditions of measurement.

The extent of natural heterogeneity within a given cell population or tissue sample can also be established using AFM. An AFM apparatus adapted for use in living brain tissue, for example, has been used to demonstrate that the rat hippocampus is heterogeneous, and that hippocampal subregions are associated with

different elastic moduli (Elkin et al., 2007). The wound healing process has also been characterized using AFM, and the leading edge of the wound was found to exhibit a spatially limited increase in stiffness to recruit fibroblasts to the wound site. This localized peak is created by cytoskeletal changes in the cells of the wound edge, and disappears if the expression of the actin fiber-regulating protein RhoA is disabled, resulting in a lack of fibroblastic recruitment to the site of injury (Wagh et al., 2008). In addition to tissues, an individual cell can also be analyzed to identify distinct regions on its surface: Scheuring et al. have characterized the mechanisms used by red blood cells to contort during their passage through blood vessels, utilizing a method in which the function of known structural proteins are altered and the resultant changes on the cell surface are measured to map these proteins onto the mechanically heterogeneous regions present on the erythrocyte (Picas et al., 2013). The addition of MgATP was utilized to elicit changes on the membrane elements on the extracellular ("outwards") and cytoplasmic ("inwards") sides of the erythrocyte, which behaved in two distinct ways and therefore allowed the detailed characterization of membrane structures and molecular compositions on both sides.

In addition to characterizing the structure of previously deposited matrix microenvironments, AFM can also determine how cellular exudates are secreted outside cells, especially with regards to the membrane budding and fusion events that occur during the secretion process. Research in this direction focuses mostly on cells involved in the secretion of hormones or digestive fluids, such as pancreatic acinar cells (Schneider et al., 1997b) or growth hormone (GH)-secreting cells (Cho et al., 2002). Secretion in acinar cells was found to depend on large (500–2000 nm) apical "pits" that contain 3–20 smaller (100–180 nm) "depressions" or "fusion pores", the diameters of which increase during amylase secretion (Fig. 8). Similar pits and depressions were also present in GH-secreting cells, and the existence of GH within these structures was confirmed using gold-tagged GH antibodies, demonstrating that the depressions were secretory in nature. A combination of atomic force microscopy and confocal microscopy was also used to demonstrate that the secretory vesicle swelling process is regulated by a GTP-binding protein (Jena et al., 1997).

5. Future directions

AFM is a versatile technique and can be used in the mechanical characterization of a broad range of biomaterials, ranging from single molecules to bulk tissues. Its nanometer-scale resolution allows the direct observation of proteins, nucleic acids and other biologically important molecules, while its ability to characterize material stiffness in liquids is a crucial advantage for investigating the natural mechanical environment of cells. However, the methods used for the preparation of biological samples for AFM imaging are highly diverse and may alter the mechanical properties of biomaterials. Environmental conditions such as temperature and buffer salinity can alter the response of cells to mechanical stimuli, while fixation and immobilization protocols may directly change the chemical composition of the treated cells. These effects in turn make it difficult to compare results between studies performed under different conditions. While countermeasures, such as liquid cells which supply the environment normally experienced by mammalian cells in cell culture, have been developed, a great deal of process optimization and standardization is still necessary for AFM to truly emerge as a biological tool.

Nevertheless, the mechanical environment of cells remains largely unexplored, and AFM is an ideal method for characterizing the behaviors of cells and tissues under close-to-natural conditions. The technique will no doubt remain indispensable for studying the mechanical components of signaling pathways and the effect of

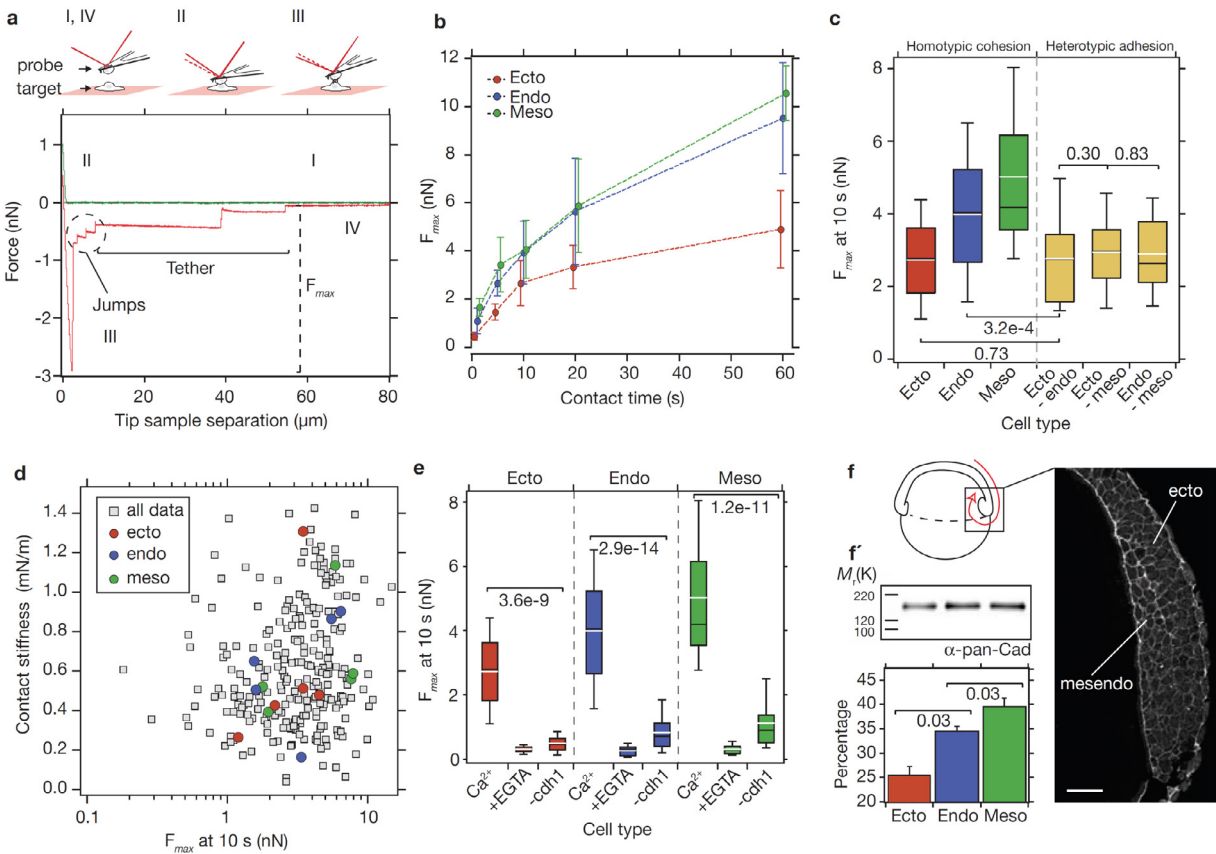


Fig. 7. Endo- and mesodermal cells of the developing zebrafish embryo preferentially adhere to cells sharing the same germ layer in a cadherin-dependent manner. Adhesive forces between two cells can be measured by attaching one cell to the probe (a). Endo- and mesodermal cells exhibit stronger homotypic adhesion compared to ectodermal cells, and heterotypic adhesion is generally weaker than endoderm–endoderm and mesoderm–mesoderm interactions (b and c, d used as control to ensure contact stiffness didn't account for the differences observed). Calcium depletion and suppression of cadherin blocks the observed effects, and cadherin expression is higher in endo- and mesodermal cells, suggesting that adhesion is cadherin-dependent (e, f). Replicated with permission from Krieg et al. (2008a).

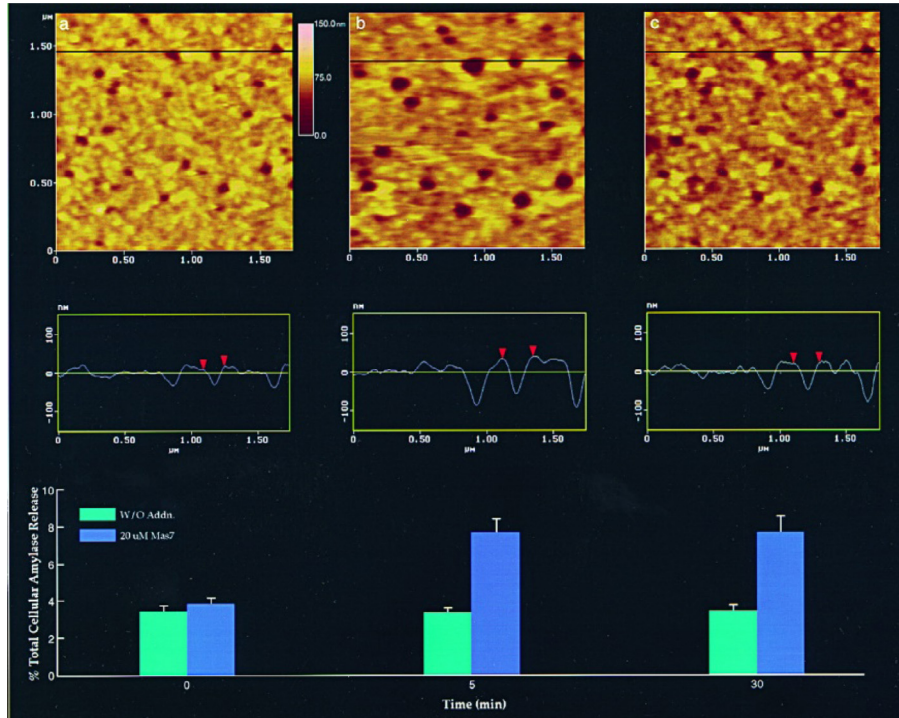


Fig. 8. Induced secretion of amylase from acinar cells of the pancreas, showing “depressions” in a single “pit” (a) and their secretory responses 5 min (b) and 30 min (c) after simulation by the secretion-stimulating peptide Mas7. Secretion is associated with increases in the diameters and depths of the secretory depressions. Replicated with permission from Schneider et al. (1997a).

physical signals on metabolic functions under normal and disease states, which is an area that has remained largely uninvestigated until now, for lack of adequate methods of analysis.

References

- Acerbi, I., Cassereau, L., Dean, I., Shi, Q., Au, A., Park, C., Chen, Y.Y., Liphardt, J., Hwang, E.S., Weaver, V.M., 2015. Human breast cancer invasion and aggression correlates with ECM stiffening and immune cell infiltration. *Integr. Biol. (Camb.)*, <http://dx.doi.org/10.1039/c5ib00040h>.
- Allen, S., Chen, X.Y., Davies, J., Davies, M.C., Dawkes, A.C., Edwards, J.C., Roberts, C.J., Sefton, J., Tendler, S.J.B., Williams, P.M., 1997. Detection of antigen-antibody binding events with the atomic force microscope. *Biochemistry* 36 (24), 7457–7463, <http://dx.doi.org/10.1021/Bi962531z>.
- Ando, T., Uchihashi, T., Koderu, N., 2013. High-speed AFM and applications to biomolecular systems. *Annu. Rev. Biophys.* 42, 393–414, <http://dx.doi.org/10.1146/annurev-biophys-083012-130324>.
- Arnold, J.W., Bailey, G.W., 2000. Surface finishes on stainless steel reduce bacterial attachment and early biofilm formation: scanning electron and atomic force microscopy study. *Poultry Sci.* 79 (12), 1839–1845.
- Auerbach, I.D., Sorensen, C., Hansma, H.G., Holden, P.A., 2000. Physical morphology and surface properties of unsaturated *Pseudomonas putida* biofilms. *J. Bacteriol.* 182 (13), 3809–3815, <http://dx.doi.org/10.1128/JB.182.13.3809-3815.2000>.
- Bakker, D., Huijs, F., de Vries, J., Klijnstra, J., Busscher, H., van der Mei, H., 2003. Bacterial deposition to fluoridated and non-fluoridated polyurethane coatings with different elastic modulus and surface tension in a parallel plate and a stagnation point flow chamber. *Colloids Surf. B* 32 (3), 179–190, [http://dx.doi.org/10.1016/S0927-7765\(03\)00159-0](http://dx.doi.org/10.1016/S0927-7765(03)00159-0).
- Beckmann, M., Venkataraman, S., Doktycz, M., Nataro, J., Sullivan, C., Morrell-Falvey, J., Allison, D., 2006. Measuring cell surface elasticity on enteroaggregative *Escherichia coli* wild type and dispersin mutant by AFM. *Ultramicroscopy* 106 (8–9), 695–702, <http://dx.doi.org/10.1016/j.ultramic.2006.02.006>.
- Beech, I.B., Smith, J.R., Steele, A.A., Penegar, I., Campbell, S.A., 2002. The use of atomic force microscopy for studying interactions of bacterial biofilms with surfaces. *Colloid Surf. B* 23 (2–3), 231–247.
- Berdyyeva, T.K., Woodworth, C.D., Sokolov, I., 2005a. Human epithelial cells increase their rigidity with ageing *in vitro*: direct measurements. *Phys. Med. Biol.* 50 (1), 81–92.
- Berdyyeva, T., Woodworth, C.D., Sokolov, I., 2005b. Visualization of cytoskeletal elements by the atomic force microscope. *Ultramicroscopy* 102 (3), 189–198.
- Berquand, A., Mingeot-Leclercq, M., Dufrene, Y., 2004. Real-time imaging of drug-membrane interactions by atomic force microscopy. *Biochim. Biophys. Acta* 1664 (2), 198–205, <http://dx.doi.org/10.1016/j.bbapam.2004.05.010>.
- Best, R.B., Li, B., Steward, A., Daggett, V., Clarke, J., 2001. Can non-mechanical proteins withstand force? Stretching barnase by atomic force microscopy and molecular dynamics simulation. *Biophys. J.* 81 (4), 2344–2356.
- Bosnakovski, D., Mizuno, M., Kim, G., Takagi, S., Okumura, M., Fujinaga, T., 2006. Chondrogenic differentiation of bovine bone marrow mesenchymal stem cells (MSCs) in different hydrogels: influence of collagen type II extracellular matrix on MSC chondrogenesis. *Biotechnol. Bioeng.* 93 (6), 1152–1163.
- Bowen, W., Fenton, A., Lovitt, R., Wright, C., 2002. The measurement of *Bacillus mycoides* spore adhesion using atomic force microscopy, simple counting methods, and a spinning disk technique. *Biotechnol. Bioeng.* 79 (2), 170–179, <http://dx.doi.org/10.1002/bit.10321>.
- Bozec, L., de Groot, J., Odlyha, M., Nicholls, B., Nesbitt, S., Flanagan, A., Horton, M., 2005. Atomic force microscopy of collagen structure in bone and dentine revealed by osteoclastic resorption. *Ultramicroscopy* 105 (1–4), 79–89, <http://dx.doi.org/10.1016/j.ultramic.2005.06.021>.
- Braet, F., Rotsch, C., Wisse, E., Radmacher, M., 1998. Comparison of fixed and living liver endothelial cells by atomic force microscopy. *Appl. Phys. A* 66, S575–S578, <http://dx.doi.org/10.1007/s003390051204>.
- Butt, H.J., Downing, K.H., Hansma, P.K., 1990. Imaging the membrane-protein bacteriorhodopsin with the atomic force microscope. *Biophys. J.* 58 (6), 1473–1480.
- Canetta, E., Riches, A., Borger, E., Herrington, S., Dholakia, K., Adya, A.K., 2014. Discrimination of bladder cancer cells from normal urothelial cells with high specificity and sensitivity: combined application of atomic force microscopy and modulated Raman spectroscopy. *Acta Biomater.* 10 (5), 2043–2055, <http://dx.doi.org/10.1016/j.actbio.2013.12.057>.
- Carvalho, F.A., Martins, I.C., Santos, N.C., 2013. Atomic force microscopy and force spectroscopy on the assessment of protein folding and functionality. *Arch. Biochem. Biophys.* 531 (1–2), 116–127, <http://dx.doi.org/10.1016/j.abb.2012.11.007>, S0003-9861(12)00400-6[pii].
- Chaw, K.C., Manimaran, M., Tay, F.E.H., 2005. Role of silver ions in destabilization of intermolecular adhesion forces measured by atomic force microscopy in *Staphylococcus epidermidis* biofilms. *Antimicrob. Agents Chemother.* 49 (12), 4853–4859, <http://dx.doi.org/10.1128/Aac.49.12.4853-4859.2005>.
- Cho, S.J., Jeftinija, K., Glavaski, A., Jeftinija, S., Jena, B.P., Anderson, L.L., 2002. Structure and dynamics of the fusion pores in live GH-secreting cells revealed using atomic force microscopy. *Endocrinology* 143 (3), 1144–1148.
- Cohen, S.R., Kalfon-Cohen, E., 2013. Dynamic nanoindentation by instrumented nanoindentation and force microscopy: a comparative review. *Beilstein J. Nanotechnol.* 4, 815–833, <http://dx.doi.org/10.3762/bjnano.4.93>.
- Connelly, L., Jang, H., Arce, F.T., Capone, R., Kotler, S.A., Ramachandran, S., Kagan, B.L., Nussinov, R., Lal, R., 2012. Atomic force microscopy and MD simulations reveal pore-like structures of all-D-enantiomer of Alzheimer's beta-amyloid peptide: relevance to the ion channel mechanism of AD pathology. *J. Phys. Chem. B* 116 (5), 1728–1735.
- Costa, K.D., 2003. Single-cell elastography: probing for disease with the atomic force microscope. *Dis. Markers* 19 (2–3), 139–154.
- Cross, S.E., Jin, Y.S., Rao, J., Gimzewski, J.K., 2007. Nanomechanical analysis of cells from cancer patients. *Nat. Nanotechnol.* 2 (12), 780–783, <http://dx.doi.org/10.1038/nano.2007.388>.
- Cross, S.E., Jin, Y.S., Lu, Q.Y., Rao, J.Y., Gimzewski, J.K., 2011. Green tea extract selectively targets nanomechanics of live metastatic cancer cells. *Nanotechnology* 22 (21), <http://dx.doi.org/10.1088/0957-4448/22/21/215101> (Artn 215101).
- Dammer, U., Popescu, O., Wagner, P., Anselmetti, D., Guntherodt, H.J., Misevic, G.N., 1995. Binding strength between cell-adhesion proteoglycans measured by atomic-force microscopy. *Science* 267 (5201), 1173–1175, <http://dx.doi.org/10.1126/science.7855599>.
- Danino, D., 2008. Advances in atomic force microscopy investigations of biomolecules. *Curr. Opin. Colloid Int.* 13 (5), 315, <http://dx.doi.org/10.1016/j.cocis.2008.07.001>.
- Darling, E., Zauscher, S., Guilak, F., 2006. Viscoelastic properties of zonal articular chondrocytes measured by atomic force microscopy. *Osteoarthritis Cartilage* 14 (6), 571–579, <http://dx.doi.org/10.1016/j.joca.2005.12.003>.
- Darling, E.M., Topel, M., Zauscher, S., Vail, T.P., Guilak, F., 2008. Viscoelastic properties of human mesenchymally-derived stem cells and primary osteoblasts, chondrocytes, and adipocytes. *J. Biomech.* 41 (2), 454–464, <http://dx.doi.org/10.1016/j.jbiomech.2007.06.019>.
- da Silva, A., Teschke, O., 2005. Dynamics of the antimicrobial peptide PGLa action on *Escherichia coli* monitored by atomic force microscopy. *World J. Microbiol. Biotechnol.* 21 (6–7), 1103–1110.
- Davies, D.G., Parsek, M.R., Pearson, J.P., Iglesias, B.H., Costerton, J.W., Greenberg, E.P., 1998. The involvement of cell-to-cell signals in the development of a bacterial biofilm. *Science* 280 (5361), 295–298, <http://dx.doi.org/10.1126/science.280.5361.295>.
- Discher, D.E., Janmey, P., Wang, Y.L., 2005. Tissue cells feel and respond to the stiffness of their substrate. *Science* 310 (5751), 1139–1143.
- Discher, D.E., 2006. BIOT 463-Matrix elasticity is sensed with non-muscle myosin II and directs stem cell lineage specification. *Abstr. Pap. Am. Chem. Soc.* 232.
- Docheva, D., Padula, D., Popov, C., Mutschler, W., Clausen-Schaumann, H., Schieker, M., 2008. Researching into the cellular shape, volume and elasticity of mesenchymal stem cells, osteoblasts and osteosarcoma cells by atomic force microscopy. *J. Cell. Mol. Med.* 12 (2), 537–552, <http://dx.doi.org/10.1111/j.1582-4934.2007.00138.x>.
- Doktycz, M.J., Sullivan, C.J., Hoyt, P.R., Pelletier, D.A., Wu, S., Allison, D.P., 2003. AFM imaging of bacteria in liquid media immobilized on gelatin coated mica surfaces. *Ultramicroscopy* 97 (1–4), 209–216, [http://dx.doi.org/10.1016/S0304-3991\(03\)00045-7](http://dx.doi.org/10.1016/S0304-3991(03)00045-7).
- Dorobantu, L.S., Goss, G.G., Burrell, R.E., 2012. Atomic force microscopy: a nanoscopic view of microbial cell surfaces. *Micron* 43 (12), 1312–1322, <http://dx.doi.org/10.1016/j.micron.2012.05.005>, S0968-4328(12)00156-4[pii].
- Dufour, D., Levesque, C.M., 2013. Bacterial behaviors associated with the quorum-sensing peptide pheromone ('alarmone') in streptococci. *Fut. Microbiol.* 8 (5), 593–605, <http://dx.doi.org/10.2217/fmb.13.23>.
- Dulinska, I., Targosz, M., Strojny, W., Lekka, M., Czuba, P., Balwierz, W., Szymonski, M., 2006. Stiffness of normal and pathological erythrocytes studied by means of atomic force microscopy. *J. Biochem. Biophys. Methods* 66 (1–3), 1–11, <http://dx.doi.org/10.1016/j.jbbm.2005.11.003>.
- Ebner, A., Wildling, L., Kamruzzahan, A.S., Rankl, C., Wruss, J., Hahn, C.D., Holzl, M., Zhu, R., Kienberger, F., Blaas, D., Hinterdorfer, P., Gruber, H.J., 2007. A new, simple method for linking of antibodies to atomic force microscopy tips. *Biconjugal. Chem.* 18 (4), 1176–1184, <http://dx.doi.org/10.1021/bc070030s>.
- Elkin, B.S., Azeloglu, E.U., Costa, K.D., Morrison, B., 2007. Mechanical heterogeneity of the rat hippocampus measured by atomic force microscope indentation. *J. Neurotrauma* 24 (5), 812–822, <http://dx.doi.org/10.1089/neu.2006.0169>.
- Engler, A.J., Griffin, M.A., Sen, S., Bonnetmann, C.G., Sweeney, H.L., Discher, D.E., 2004. Myotubes differentiate optimally on substrates with tissue-like stiffness: pathological implications for soft or stiff microenvironments. *J. Cell Biol.* 166 (6), 877–887, <http://dx.doi.org/10.1083/jcb.200405004>.
- Evans, N.D., Minelli, C., Gentleman, E., LaPointe, V., Patankar, S.N., Kallivretaki, M., Chen, X.Y., Roberts, C.J., Stevens, M.M., 2009. Substrate stiffness affects early differentiation events in embryonic stem cells. *Eur. Cells Mater.* 18, 1–14.
- Fang, H., Chan, K., Xu, L., 2000. Quantification of bacterial adhesion forces using atomic force microscopy (AFM). *J. Microbiol. Methods* 40 (1), 89–97, [http://dx.doi.org/10.1016/S0167-7012\(99\)00137-2](http://dx.doi.org/10.1016/S0167-7012(99)00137-2).
- Fantner, G.E., Barbero, R.J., Gray, D.S., Belcher, A.M., 2010a. Kinetics of antimicrobial peptide activity measured on individual bacterial cells using high-speed atomic force microscopy. *Nat. Nanotechnol.* 5 (4), 280–285, <http://dx.doi.org/10.1038/nano.2010.29>.
- Fantner, G.E., Barbero, R.J., Gray, D.S., Belcher, A.M., 2010b. Kinetics of antimicrobial peptide activity measured on individual bacterial cells using high-speed atomic force microscopy. *Nat. Nanotechnol.* 5 (4), 280–285, <http://dx.doi.org/10.1038/nano.2010.29>.
- Fernandes, J.C., Eaton, P., Gomes, A.M., Pintado, M.E., Malcata, F.X., 2009. Study of the antibacterial effects of chitosans on *Bacillus cereus* (and its spores) by

- atomic force microscopy imaging and nanoindentation.** *Ultramicroscopy* 109 (8), 854–860.
- Florin, E.L., Rief, M., Lehmann, H., Ludwig, M., Dornmair, C., Moy, V.T., Gaub, H.E., 1995. Sensing specific molecular interactions with the atomic-force microscope. *Biosens. Bioelectron.* 10 (9–10), 895–901, [http://dx.doi.org/10.1016/0956-5663\(95\)99227-C](http://dx.doi.org/10.1016/0956-5663(95)99227-C).
- Fotiadis, D., Liang, Y., Filipek, S., Saperstein, D.A., Engel, A., Palczewski, K., 2003. **Atomic-force microscopy: rhodopsin dimers in native disc membranes.** *Nature* 421 (6919), 127–128.
- Francius, G., Lebeer, S., Alsteens, D., Wildling, L., Gruber, H.J., Hols, P., De Keersmaecker, S., Vanderleyden, J., Dufrene, Y.F., 2008. Detection, localization, and conformational analysis of single polysaccharide molecules on live bacteria. *ACS Nano* 2 (9), 1921–1929, <http://dx.doi.org/10.1021/Nn800341b>.
- Fuhrmann, A., Staunton, J.R., Nandakumar, V., Banyai, N., Davies, P.C.W., Ros, R., 2011. **AFM stiffness nanotomography of normal, metaplastic and dysplastic human esophageal cells.** *Phys. Biol.* 8 (1).
- Giessibl, F.J., 2003. Advances in atomic force microscopy. *Rev. Mod. Phys.* 75 (3), 949–983, <http://dx.doi.org/10.1103/RevModPhys.75.949>.
- Gonzalez-Cruz, R.D., Fonseca, V.C., Darling, E.M., 2012. Cellular mechanical properties reflect the differentiation potential of adipose-derived mesenchymal stem cells. *Proc. Natl. Acad. Sci. U. S. A.* 109 (24), E1523–E1529, <http://dx.doi.org/10.1073/pnas.1120349109>.
- Grandbois, M., Dettmann, W., Benoit, M., Gaub, H.E., 2000. **Affinity imaging of red blood cells using an atomic force microscope.** *J. Histochem. Cytochem.* 48 (5), 719–724.
- Guhados, G., Wan, W., Hutter, J., 2005. Measurement of the elastic modulus of single bacterial cellulose fibers using atomic force microscopy. *Langmuir* 21 (14), 6642–6646, <http://dx.doi.org/10.1021/la0504311>.
- Guilak, F., Cohen, D.M., Estes, B.T., Gimble, J.M., Liedtke, W., Chen, C.S., 2009. **Control of stem cell fate by physical interactions with the extracellular matrix.** *Cell Stem Cell* 5 (1), 17–26.
- Gyورvay, E.S., Stein, O., Pum, D., Sleytr, U.B., 2003a. **Self-assembly and recrystallization of bacterial S-layer proteins at silicon supports imaged in real time by atomic force microscopy.** *J. Microsc. Oxford* 212, 300–306.
- Gyورvay, E., Stein, O., Pum, D., Sleytr, U., 2003b. Self-assembly and recrystallization of bacterial S-layer proteins at silicon supports imaged in real time by atomic force microscopy. *J. Microsc. Oxford* 212, 300–306, <http://dx.doi.org/10.1111/j.1365-2818.2003.01270.x>.
- Haga, H., Sasaki, S., Kawabata, K., Ito, E., Ushiki, T., Sambongi, T., 2000. Elasticity mapping of living fibroblasts by AFM and immunofluorescence observation of the cytoskeleton. *Ultramicroscopy* 82 (1–4), 253–258, [http://dx.doi.org/10.1016/S0304-3991\(99\)00157-6](http://dx.doi.org/10.1016/S0304-3991(99)00157-6).
- Han, T., Williams, J.M., Beebe, T.P., 1995. Chemical Bonds studied with functionalized atomic-force microscopy tips. *Anal. Chim. Acta* 307 (2–3), 365–376, [http://dx.doi.org/10.1016/0003-2670\(94\)00671-8](http://dx.doi.org/10.1016/0003-2670(94)00671-8).
- Hansma, H.G., Laney, D.E., Bezanilla, M., Sinsheimer, R.L., Hansma, P.K., 1995. **Applications for atomic-force microscopy of DNA.** *Biophys. J.* 68 (5), 1672–1677.
- Hansma, H.G., Revenko, I., Kim, K., Laney, D.E., 1996. Atomic force microscopy of long and short double-stranded, single-stranded and triple-stranded nucleic acids. *Nucleic Acids Res.* 24 (4), 713–720, <http://dx.doi.org/10.1093/Nar/24.4.713>.
- Harimawan, A., Rajasekar, A., Ting, Y.P., 2011. Bacteria attachment to surfaces – AFM force spectroscopy and physicochemical analyses. *J. Colloid Interface Sci.* 364 (1), 213–218, <http://dx.doi.org/10.1016/j.jcis.2011.08.021>.
- Harper, J.D., Wong, S.S., Lieber, C.M., Lansbury, P.T., 1997. Observation of metastable A beta amyloid protofibrils by atomic force microscopy. *Chem. Biol.* 4 (2), 119–125, [http://dx.doi.org/10.1016/S1074-5521\(97\)90255-6](http://dx.doi.org/10.1016/S1074-5521(97)90255-6).
- Huang, G.Y., Wang, L., Wang, S.Q., Han, Y.L., Wu, J.H., Zhang, Q.C., Xu, F., Lu, T.J., 2012. **Engineering three-dimensional cell mechanical microenvironment with hydrogels.** *Biofabrication* 4 (4).
- Iyer, S., Gaikwad, R.M., Subba-Rao, V., Woodworth, C.D., Sokolov, I., 2009. Atomic force microscopy detects differences in the surface brush of normal and cancerous cells. *Nat. Nanotechnol.* 4 (6), 389–393, <http://dx.doi.org/10.1038/Nano.2009.77>.
- Jena, B., Schneider, S., Geibel, J., Webster, P., Oberleithner, H., Sritharan, K., 1997. G(i) regulation of secretory vesicle swelling examined by atomic force microscopy. *Proc. Natl. Acad. Sci. U. S. A.* 94 (24), 13317–13322, <http://dx.doi.org/10.1073/pnas.94.24.13317>.
- Jaenisch, R., Bird, A., 2003. Epigenetic regulation of gene expression: how the genome integrates intrinsic and environmental signals. *Nat. Genet.* 33 (Suppl.), 245–254, <http://dx.doi.org/10.1038/ng1089> (ng1089 [iii]).
- Jin, H., Xing, X., Zhao, H., Chen, Y., Huang, X., Ma, S., Ye, H., Cai, J., 2010. Detection of erythrocytes influenced by aging and type 2 diabetes using atomic force microscope. *Biochem. Biophys. Res. Commun.* 391 (4), 1698–1702, <http://dx.doi.org/10.1016/j.bbrc.2009.12.133>.
- Johnson, A.W., 2013. Eating beyond metabolic need: how environmental cues influence feeding behavior. *Trends Neurosci.* 36 (2), 101–109, <http://dx.doi.org/10.1016/j.tins.2013.01.002>, S0166-2236(13)00005-2[pii].
- Kamruzzahan, A.S., Ebner, A., Wildling, L., Kienberger, F., Riener, C.K., Hahn, C.D., Pollheimer, P.D., Winklebauer, P., Holzl, M., Lackner, B., Schorkl, D.M., Hinterdorfer, P., Gruber, H.J., 2006. Antibody linking to atomic force microscope tips via disulfide bond formation. *Bioconjug. Chem.* 17 (6), 1473–1481, <http://dx.doi.org/10.1021/bc060252a>.
- Kodera, N., Yamamoto, D., Ishikawa, R., Ando, T., 2010. Video imaging of walking myosin V by high-speed atomic force microscopy. *Nature* 468 (7320), 72+, <http://dx.doi.org/10.1038/Nature09450>.
- Kowalewski, T., Holtzman, D.M., 1999. In situ atomic force microscopy study of Alzheimer's beta-amyloid peptide on different substrates: new insights into mechanism of beta-sheet formation. *Proc. Natl. Acad. Sci. U. S. A.* 96 (7), 3688–3693, <http://dx.doi.org/10.1073/pnas.96.7.3688>.
- Krieg, M., Arboleda-Estudillo, Y., Puech, P., Kafer, J., Graner, F., Muller, D., Heisenberg, C., 2008a. Tensile forces govern germ-layer organization in zebrafish. *Nat. Cell Biol.* 10 (4), <http://dx.doi.org/10.1038/ncb1705>, 429–U122.
- Krieg, M., Arboleda-Estudillo, Y., Puech, P.H., Kafer, J., Graner, F., Muller, D.J., Heisenberg, C.P., 2008b. **Tensile forces govern germ-layer organization in zebrafish.** *Nat. Cell Biol.* 10 (4), 429–U122.
- Kuznetsov, Y.G., McPherson, A., 2011. **Atomic force microscopy in imaging of viruses and virus-infected cells.** *Microbiol. Mol. Biol. Rev.* 75 (2), 268–285.
- Lal, R., John, S.A., 1994. **Biological applications of atomic-force microscopy.** *Am. J. Physiol.* 266 (1), C1–&.
- Lasalvia, M., D'Antonio, P., Perna, G., Capozzi, V., Mariggio, M., Perrone, D., Gallo, C., Quartucci, G., Lo Muzio, L., 2015. Discrimination of different degrees of oral squamous cell carcinoma by means of Raman microspectroscopy and atomic force microscopy. *Anal. Methods* 7 (2), 699–707, <http://dx.doi.org/10.1039/c4ay02282c>.
- Last, J., Liliensiek, S., Nealey, P., Murphy, C., 2009. Determining the mechanical properties of human corneal basement membranes with atomic force microscopy. *J. Struct. Biol.* 167 (1), 19–24, <http://dx.doi.org/10.1016/j.jsb.2009.03.012>.
- Laurent, V.M., Duperray, A., Sundar Rajan, V., Verdier, C., 2014. Atomic force microscopy reveals a role for endothelial cell ICAM-1 expression in bladder cancer cell adherence. *PLoS One* 9 (5), e98034, <http://dx.doi.org/10.1371/journal.pone.0098034>.
- Lee, G.U., Kidwell, D.A., Colton, R.J., 1994. Sensing discrete streptavidin biotin interactions with atomic-force microscopy. *Langmuir* 10 (2), 354–357, <http://dx.doi.org/10.1021/La00014a003>.
- Lee, C.K., Wang, Y.M., Huang, L.S., Lin, S.M., 2007. Atomic force microscopy: determination of unbinding force, off rate and energy barrier for protein-ligand interaction. *Micron* 38 (5), 446–461, <http://dx.doi.org/10.1016/j.micron.2006.06.014>.
- Lekka, M., Gil, D., Pogoda, K., Dulinska-Litewka, J., Jach, R., Gostek, J., Klymenko, O., Prauzner-Beczkicki, S., Stachura, Z., Wilkowska-Zuber, J., Okon, K., Laidler, P., 2012. Cancer cell detection in tissue sections using AFM. *Arch. Biochem. Biophys.* 518 (2), 151–156, <http://dx.doi.org/10.1016/j.abb.2011.12.013>.
- Li, H.B., Carrion-Vazquez, M., Oberhauser, A.F., Marszalek, P., Fernandez, J.M., 2003. **Stretching single molecules into novel conformations using the atomic force microscope.** *Abstr. Pap. Am. Chem. Soc.* 225, U685.
- Li, Q., Lee, G., Ong, C., Lim, C., 2008. AFM indentation study of breast cancer cells. *Biochem. Biophys. Res. Commun.* 374 (4), 609–613, <http://dx.doi.org/10.1016/j.bbrc.2008.07.078>.
- Lieber, S., Aubry, N., Pain, J., Diaz, G., Kim, S., Vatner, S., 2004a. Aging increases stiffness of cardiac myocytes measured by atomic force microscopy nanoindentation. *Am. J. Physiol. Heart Circ. Physiol.* 287 (2), H645–H651, <http://dx.doi.org/10.1152/ajpheart.00564.2003>.
- Lieber, S.C., Aubry, N., Pain, J., Diaz, G., Kim, S.J., Vatner, S.F., 2004b. Aging increases stiffness of cardiac myocytes measured by atomic force microscopy nanoindentation. *Am. J. Physiol. Heart Circ. Physiol.* 287 (2), H645–H651, <http://dx.doi.org/10.1152/ajpheart.00564.2003>.
- Liu, Z., Li, Z., Zhou, H., Wei, G., Song, Y., Wang, L., 2005. Imaging DNA molecules on mica surface by atomic force microscopy in air and in liquid. *Microsc. Res. Tech.* 66 (4), 179–185, <http://dx.doi.org/10.1002/jemt.20156>.
- Lombardo, M., Lombardo, G., Carbone, G., De Santo, M., Barberi, R., Serrao, S., 2012. Biomechanics of the anterior human corneal tissue investigated with atomic force microscopy. *Invest. Ophthalmol. Vis. Sci.* 53 (2), 1050–1057, <http://dx.doi.org/10.1167/iovs.11-8720>.
- Lopez, J.I., Kang, I., You, W.K., McDonald, D.M., Weaver, V.M., 2011. In situ force mapping of mammary gland transformation. *Integr. Biol. (Camb.)* 3 (9), 910–921, <http://dx.doi.org/10.1039/c1ib00043h>.
- Mao, C.D., Sun, W.Q., Seeman, N.C., 1999. Designed two-dimensional DNA Holliday junction arrays visualized by atomic force microscopy. *J. Am. Chem. Soc.* 121 (23), 5437–5443, <http://dx.doi.org/10.1021/Ja9900398>.
- Mao, Y., Sun, Q., Wang, X., Ouyang, Q., Han, L., Jiang, L., Han, D., 2009. In vivo nanomechanical imaging of blood-vessel tissues directly in living mammals using atomic force microscopy. *Appl. Phys. Lett.* 95 (1), <http://dx.doi.org/10.1063/1.3167546>.
- Mathur, A., Collinsworth, A., Reichert, W., Kraus, W., Truskey, G., 2001. Endothelial, cardiac muscle and skeletal muscle exhibit different viscous and elastic properties as determined by atomic force microscopy. *J. Biomech.* 34 (12), 1545–1553, [http://dx.doi.org/10.1016/S0021-9290\(01\)00149-X](http://dx.doi.org/10.1016/S0021-9290(01)00149-X).
- Mecke, A., Lee, D.K., Ramamoorthy, A., Orr, B.G., Holl, M.M.B., 2005. Membrane thinning due to antimicrobial peptide binding: an atomic force microscopy study of MSI-78 in lipid bilayers. *Biophys. J.* 89 (6), 4043–4050, <http://dx.doi.org/10.1529/biophysj.105.062596>.
- Meincken, A., Holroyd, D.L., Rautenbach, M., 2005. **Atomic force microscopy study of the effect of antimicrobial peptides on the cell envelope of Escherichia coli.** *Antimicrob. Agents Chemother.* 49 (10), 4085–4092.
- Mou, J.X., Yang, J., Shao, Z.F., 1995. **Atomic-force microscopy of cholera-toxin B-oligomers bound to bilayers of biologically relevant lipids.** *J. Mol. Biol.* 248 (3), 507–512.

- Muller, D.J., Dufrene, Y.F., 2008. Atomic force microscopy as a multifunctional molecular toolbox in nanobiotechnology. *Nat. Nanotechnol.* 3 (5), 261–269, <http://dx.doi.org/10.1038/nnano.2008.100>.
- Muller, D.J., Baumeister, W., Engel, A., 1999. Controlled unzipping of a bacterial surface layer with atomic force microscopy. *Proc. Natl. Acad. Sci. U.S.A.* 96 (23), 13170–13174, <http://dx.doi.org/10.1073/pnas.96.23.13170>.
- Muller, D., Janovjak, H., Lehto, T., Kuerschner, L., Anderson, K., 2002. Observing structure, function and assembly of single proteins by AFM. *Prog. Biophys. Mol. Biol.* 79 (1–3), 1–43, [http://dx.doi.org/10.1016/S0079-6107\(02\)00009-3](http://dx.doi.org/10.1016/S0079-6107(02)00009-3).
- Nagao, E., Nishijima, H., Akita, S., Nakayama, Y., Dvorak, J.A., 2000. The cell biological application of carbon nanotube probes for atomic force microscopy: comparative studies of malaria-infected erythrocytes. *J. Electron Microsc. (Tokyo)* 49 (3), 453–458.
- Neuman, K.C., Nagy, A., 2008. Single-molecule force spectroscopy: optical tweezers, magnetic tweezers and atomic force microscopy. *Nat. Methods* 5 (6), 491–505, <http://dx.doi.org/10.1038/Nmeth.1218>.
- Oberhauser, A., Marszałek, P., Carrion-Vazquez, M., Fernandez, J., 1999. Single protein misfolding events captured by atomic force microscopy. *Nat. Struct. Biol.* 6 (11), 1025–1028.
- Oh, Y., Jo, W., Yang, Y., Park, S., 2007. Influence of culture conditions on *Escherichia coli* O157: H7 biofilm formation by atomic force microscopy. *Ultramicroscopy* 107 (10–11), 869–874, <http://dx.doi.org/10.1016/j.ultramic.2007.01.021>.
- Owens, G.K., Wise, G., 1997. Regulation of differentiation/maturation in vascular smooth muscle cells by hormones and growth factors. *Agents Actions Suppl.* 48, 3–24.
- Perry, C.C., Weatherly, M., Beale, T., Randriamahefa, A., 2009. Atomic force microscopy study of the antimicrobial activity of aqueous garlic versus ampicillin against *Escherichia coli* and *Staphylococcus aureus*. *J. Sci. Food Agric.* 89 (6), 958–964.
- Picas, L., Rico, F., Deforet, M., Scheuring, S., 2013. Structural and mechanical heterogeneity of the erythrocyte membrane reveals hallmarks of membrane stability. *ACS Nano* 7 (2), 1054–1063, <http://dx.doi.org/10.1021/Nn303824j>.
- Preiner, J., Kodera, N., Tang, J., Ebner, A., Brameshuber, M., Blaas, D., Gelmann, N., Gruber, H., Ando, T., Hinterdorfer, P., 2014. IgGs are made for walking on bacterial and viral surfaces. *Nat. Commun.* 5, <http://dx.doi.org/10.1038/ncomms5394>.
- Puech, P.H., Taubenberger, A., Ulrich, F., Krieg, M., Muller, D.J., Heisenberg, C.P., 2005. Measuring cell adhesion forces of primary gastrulating cells from zebrafish using atomic force microscopy. *J. Cell Sci.* 118 (18), 4199–4206.
- Pyne, A., Thompson, R., Leung, C., Roy, D., Hoogenboom, B.W., 2014. Single-molecule reconstruction of oligonucleotide secondary structure by atomic force microscopy. *Small* 10 (16), 3257–3261, <http://dx.doi.org/10.1002/smll.201400265>.
- Rabinovich, Y., Esayanur, M., Daosukho, S., Byer, K., El-Shall, H., Khan, S., 2005. Atomic force microscopy measurement of the elastic properties of the kidney epithelial cells. *J. Colloid Interface Sci.* 285 (1), 125–135, <http://dx.doi.org/10.1016/j.jcis.2004.11.041>.
- Raman, A., Trigueros, S., Cartagena, A., Stevenson, A.P.Z., Susilo, M., Nauman, E., Contera, S.A., 2011. Mapping nanomechanical properties of live cells using multi-harmonic atomic force microscopy. *Nat. Nanotechnol.* 6 (12), 809–814, <http://dx.doi.org/10.1038/NNano.2011.186>.
- Ravichandran, K.S., 2003. Recruitment signals from apoptotic cells: invitation to a quiet meal. *Cell* 113 (7), 817–820 (S0092867403004719[pii]).
- Razatos, A., Ong, Y., Sharma, M., Georgiou, G., 1998. Molecular determinants of bacterial adhesion monitored by atomic force microscopy. *Proc. Natl. Acad. Sci. U. S. A.* 95 (19), 11059–11064, <http://dx.doi.org/10.1073/pnas.95.19.11059>.
- Reilly, G.C., Engler, A.J., 2010. Intrinsic extracellular matrix properties regulate stem cell differentiation. *J. Biomed. Mater. Res.* 43 (1), 55–62.
- Ren, J., Huang, H., Liu, Y., Zheng, X., Zou, Q., 2015. An atomic force microscope study revealed two mechanisms in the effect of anticancer drugs on rate-dependent young's modulus of human prostate cancer cells. *PLoS One* 10 (5), <http://dx.doi.org/10.1371/journal.pone.0126107>.
- Revenko, I., Sommer, F., Minh, D.T., Garrone, R., Franc, J.M., 1994. Atomic-force microscopy study of the collagen fiber structure. *Biol. Cell* 80 (1), 67–69, [http://dx.doi.org/10.1016/0248-4900\(94\)90019-1](http://dx.doi.org/10.1016/0248-4900(94)90019-1).
- Revaikein, I., Bergsma-Schutter, W., Brisson, A., 1998. Growth of protein 2-d crystals on supported planar lipid bilayers imaged in situ by AFM. *J. Struct. Biol.* 121 (3), 356–362, <http://dx.doi.org/10.1006/jstb.1998.4003>.
- Ricca, B.L., Venugopalan, G., Fletcher, D.A., 2013. To pull or be pulled: parsing the multiple modes of mechanotransduction. *Curr. Opin. Cell Biol.* 25 (5), 558–564, <http://dx.doi.org/10.1016/j.celb.2013.06.002>, S0955-0674(13)00104-X[pii].
- Rief, M., Gautel, M., Schemmel, A., Gaub, H.E., 1998. The mechanical stability of immunoglobulin and fibronectin III domains in the muscle protein titin measured by atomic force microscopy. *Biophys. J.* 75 (6), 3008–3014.
- Rotsch, C., Radmacher, M., 2000. Drug-induced changes of cytoskeletal structure and mechanics in fibroblasts: an atomic force microscopy study. *Biophys. J.* 78 (1), 520–535.
- Sader, J., Chon, J., Mulvaney, P., 1999. Calibration of rectangular atomic force microscope cantilevers. *Rev. Sci. Instrum.* 70 (10), 3967–3969, <http://dx.doi.org/10.1063/1.1150021>.
- Schneider, S.W., Sritharan, K.C., Geibel, J.P., Oberleithner, H., Jena, B.P., 1997a. Surface dynamics in living acinar cells imaged by atomic force microscopy: identification of plasma membrane structures involved in exocytosis. *Proc. Natl. Acad. Sci. U. S. A.* 94 (1), 316–321.
- Schneider, S.W., Sritharan, K.C., Geibel, J.P., Oberleithner, H., Jena, B.P., 1997b. Surface dynamics in living acinar cells imaged by atomic force microscopy: identification of plasma membrane structures involved in exocytosis. *Proc. Natl. Acad. Sci. U. S. A.* 94 (1), 316–321.
- Shao, Z.F., Mou, J., Czajkowsky, D.M., Yang, J., Yuan, J.Y., 1996. Biological atomic force microscopy: what is achieved and what is needed. *Adv. Phys.* 45 (1), 1–86, <http://dx.doi.org/10.1080/00018739600101467>.
- Sheng, X., Ting, Y., Pehkonen, S., 2007. Force measurements of bacterial adhesion on metals using a cell probe atomic force microscope. *J. Colloid Interface Sci.* 310 (2), 661–669, <http://dx.doi.org/10.1016/j.jcis.2007.01.084>.
- Shibata-Seki, T., Tajima, K., Takahashi, H., Seki, H., Masai, J., Goto, H., Kobatake, E., Akaike, T., Itoh, N., 2015. AFM characterization of chemically treated corneal cells. *Anal. Bioanal. Chem.* 407 (9), 2631–2635, <http://dx.doi.org/10.1007/s00216-015-8473-0>.
- Stoffler, D., Goldie, K.N., Feja, B., Aeby, U., 1999. Calcium-mediated structural changes of native nuclear pore complexes monitored by time-lapse atomic force microscopy. *J. Mol. Biol.* 287 (4), 741–752.
- Stolz, M., Raiteri, R., Daniels, A.U., VanLandingham, M.R., Baschong, W., Aeby, U., 2004. Dynamic elastic modulus of porcine articular cartilage determined at two different levels of tissue organization by indentation-type atomic force microscopy. *Biophys. J.* 86 (5), 3269–3283, [http://dx.doi.org/10.1016/S0006-3495\(04\)74375-1](http://dx.doi.org/10.1016/S0006-3495(04)74375-1).
- Stolz, M., Gottardi, R., Raiteri, R., Miot, S., Martin, I., Imer, R., Staufer, U., Raducanu, A., Duggelin, M., Baschong, W., Daniels, A., Friederich, N., Aszodi, A., Aeby, U., 2009a. Early detection of aging cartilage and osteoarthritis in mice and patient samples using atomic force microscopy. *Nat. Nanotechnol.* 4 (3), 186–192, <http://dx.doi.org/10.1038/NNANO.1;2008.410>.
- Stolz, M., Gottardi, R., Raiteri, R., Miot, S., Martin, I., Imer, R., Staufer, U., Raducanu, A., Duggelin, M., Baschong, W., Daniels, A.U., Friederich, N., Aszodi, A., Aeby, U., 2009b. Early detection of aging cartilage and osteoarthritis in mice and patient samples using atomic force microscopy. *Nat. Nanotechnol.* 4 (3), 186–192, <http://dx.doi.org/10.1038/nnano.2008.410>.
- Sullivan, C., Venkataraman, S., Retterer, S., Allison, D., Doktycz, M., 2007. Comparison of the indentation and elasticity of *E-coli* and its spheroplasts by AFM. *Ultramicroscopy* 107 (10–11), 934–942, <http://dx.doi.org/10.1016/j.ultramic.2007.04.017>.
- Suo, Z.Y., Avci, R., Yang, X.H., Pascual, D.W., 2008. Efficient immobilization and patterning of live bacterial cells. *Langmuir* 24 (8), 4161–4167, <http://dx.doi.org/10.1021/la7038653>.
- Suzuki, A., Iwama, A., Miyashita, H., Nakauchi, H., Taniguchi, H., 2003. Role for growth factors and extracellular matrix in controlling differentiation of prospectively isolated hepatic stem cells. *Development* 130 (11), 2513–2524.
- Thurner, P., 2009. Atomic force microscopy and indentation force measurement of bone. *Wiley Interdiscip. Rev. Nanomed. Nanobiotechnol.* 1 (6), 624–649, <http://dx.doi.org/10.1002/wnn.56>.
- Thwaites, J.J., Surana, U.C., 1991. Mechanical-properties of *Bacillus subtilis* cell-walls – effects of removing residual culture-medium. *J. Bacteriol.* 173 (1), 197–203.
- Touhami, A., Nysten, B., Dufrene, Y., 2003. Nanoscale mapping of the elasticity of microbial cells by atomic force microscopy. *Langmuir* 19 (11), 4539–4543, <http://dx.doi.org/10.1021/la034136x>.
- Touhami, A., Jericho, M., Boyd, J., Beveridge, T., 2006. Nanoscale characterization and determination of adhesion forces of *Pseudomonas aeruginosa* Pili by using atomic force microscopy. *J. Bacteriol.* 188 (2), 370–377, <http://dx.doi.org/10.1128/JB.188.2.370-377.2006>.
- Vadillo-Rodrigues, V., Busscher, H., Norde, W., De Vries, J., Dijkstra, R., Stokroos, I., van der Mei, H., 2004. Comparison of atomic force microscopy interaction forces between bacteria and silicon nitride substrata for three commonly used immobilization methods. *Appl. Environ. Microbiol.* 70 (9), 5441–5446, <http://dx.doi.org/10.1128/AEM.70.9>.
- Vadillo-Rodriguez, V., Beveridge, T., Dutcher, J., 2008. Surface viscoelasticity of individual gram-negative bacterial cells measured using atomic force microscopy. *J. Bacteriol.* 190 (12), 4225–4232, <http://dx.doi.org/10.1128/JB.00132-08>.
- van der Aa, B., Dufrene, Y., 2002. In situ characterization of bacterial extracellular polymeric substances by AFM. *Colloids Surf. B* 23 (2–3), 173–182, [http://dx.doi.org/10.1016/S0927-7765\(01\)00229-6](http://dx.doi.org/10.1016/S0927-7765(01)00229-6).
- van der Mei, H., Busscher, H., Bos, R., de Vries, J., Boonaert, C., Dufrene, Y., 2000. Direct probing by atomic force microscopy of the cell surface softness of a fibrillated and nonfibrillated oral streptococcal strain. *Biophys. J.* 78 (5), 2668–2674.
- Volle, C., Ferguson, M., Aidala, K., Spain, E., Nunez, M., 2008. Spring constants and adhesive properties of native bacterial biofilm cells measured by atomic force microscopy. *Colloids Surf. B* 67 (1), 32–40, <http://dx.doi.org/10.1016/j.colsurfb.2008.07.021>.
- Wagh, A.A., Roan, E., Chapman, K.E., Desai, L.P., Rendon, D.A., Eckstein, E.C., Waters, C.M., 2008. Localized elasticity measured in epithelial cells migrating at a wound edge using atomic force microscopy. *Am. J. Physiol. Lung Cell. Mol. Physiol.* 295 (1), L54–60, <http://dx.doi.org/10.1152/ajplung.00475.2007>.
- Wang, J.Y., Wan, Z.F., Liu, W.M., Li, L., Ren, L., Wang, X.Q., Sun, P., Ren, L.L., Zhao, H.Y., Tu, Q., Zhang, Z.Y., Song, N., Zhang, L., 2009. Atomic force microscope study of tumor cell membranes following treatment with anti-cancer drugs. *Biosens. Bioelectron.* 25 (4), 721–727, <http://dx.doi.org/10.1016/j.bios.2009.08.011>.
- Wang, X., Wang, J., Liu, Y., Zong, H., Che, X., Zheng, W., Chen, F., Zhu, Z., Yang, D., Song, X., 2014. Alterations in mechanical properties are associated with prostate cancer progression. *Med. Oncol.* 31 (3), <http://dx.doi.org/10.1007/s12032-014-0876-9>.

- Watt, F.M., Huck, W.T., 2013. Role of the extracellular matrix in regulating stem cell fate. *Nat. Rev. Mol. Cell Biol.* 14 (8), 467–473 (nrm3620[pii]).
- Wu, Y.Z., McEwen, G.D., Harihar, S., Baker, S.M., DeWald, D.B., Zhou, A.H., 2010. BRMS1 expression alters the ultrastructural, biomechanical and biochemical properties of MDA-MB-435 human breast carcinoma cells: an AFM and Raman microspectroscopy study. *Cancer Lett.* 293 (1), 82–91, <http://dx.doi.org/10.1016/j.canlet.2009.12.016>.
- Xiong, Y., Lee, A., Suter, D., Lee, G., 2009. Topography and nanomechanics of live neuronal growth cones analyzed by atomic force microscopy. *Biophys. J.* 96 (12), 5060–5072, <http://dx.doi.org/10.1016/j.bpj.2009.03.032>.
- Yaneva, M., Kowalewski, T., Lieber, M.R., 1997. Interaction of DNA-dependent protein kinase with DNA and with Ku: biochemical and atomic-force microscopy studies. *EMBO J.* 16 (16), 5098–5112, <http://dx.doi.org/10.1093/emboj/16.16.5098>.
- Yao, X., Jericho, M., Pink, D., Beveridge, T., 1999. Thickness and elasticity of gram-negative murein sacci measured by atomic force microscopy. *J. Bacteriol.* 181 (22), 6865–6875.
- Yoo, L., Reed, J., Shin, A., Demer, J.L., 2014. Atomic force microscopy determination of Young's modulus of bovine extra-ocular tendon fiber bundles. *J. Biomech.* 47 (8), 1899–1903, <http://dx.doi.org/10.1016/j.jbiomech.2014.02.011>.
- Yuan, C.B., Furlong, J., Burgos, P., Johnston, L.J., 2002. The size of lipid rafts: an atomic force microscopy study of ganglioside GM1 domains in sphingomyelin/DOPC/cholesterol membranes. *Biophys. J.* 82 (5), 2526–2535.
- Zamir, E.A., Srinivasan, V., Perucchio, R., Taber, L.A., 2003. Mechanical asymmetry in the embryonic chick heart during looping. *Ann. Biomed. Eng.* 31 (11), 1327–1336.
- Zhao, L., Schaefer, D., Xu, H., Modi, S., LaCourse, W., Marten, M., 2005. Elastic properties of the cell wall of *Aspergillus nidulans* studied with atomic force microscopy. *Biotechnol. Progr.* 21 (1), 292–299, <http://dx.doi.org/10.1021/bp049723s>.
- Ziebarth, N., Wojcikiewicz, E., Manns, F., Moy, V., Parel, J., 2007. Atomic force microscopy measurements of lens elasticity in monkey eyes. *Mol. Vis.* 13 (52–55), 504–510.
- Zoranovic, T., Grmai, L., Bach, E.A., 2013. Regulation of proliferation, cell competition, and cellular growth by the JAK-STAT pathway. *JAKSTAT* 2 (3), e25408, <http://dx.doi.org/10.4161/jkst.25408> (2012JAKS0117R[pii]).